Project Report
EO-1-7

Earth Observing-1 Advanced Land Imager Flight Performance Assessment:

Noise and Dark Current Trending for the First 60 Days

J.A. Mendenhall and M.D. Gibbs

Lincoln Laboratory
Massachusetts Institute of Technology
Lexington, Massachusetts

1 June 2001

Prepared for the National Aeronautics and Space Administration
under Air Force Contract F19628-00-C-0002.

Abstract

Noise and dark current trending for the Earth Observing-1 Advanced Land Imager during its initial sixty days in orbit (November 21, 2000 – January 19, 2001) is presented. Data were collected with the focal plane operating nominally at 220 K. The results presented here indicate the magnitude and repeatability of the focal plane noise has been good and closely matches pre-flight calibration measurements. The magnitude of the focal plane dark current for all bands has also been good, closely matches pre-flight calibration measurements, and has excellent stability during individual observations. However, dark current level variability as high as 30 digital numbers for Bands 1p, 4, 4p, 5p, 5, 7, and the Panchromatic band has been observed from one observation to another and is not well understood at this time.

Table of Contents

List of Figures

List of Tables

1 Introduction

The Advanced Land Imager (ALI) was built at MIT Lincoln Laboratory and is meant to serve as a technology demonstration for a possible future Landsat instrument[1-5]. Two key areas of this demonstration are sustainable low noise performance and stable, repeatable dark current levels. The ALI was successfully launched into orbit aboard the Earth Observing-1 spacecraft by a Boeing Delta II rocket on November 21, 2000. This document provides detector noise and dark current trending results of the Advanced Land Imager during its first sixty days in orbit (November 21, 2000 – January 19, 2001). Data will be trended for each of the ten spectral bands and each of the four sensor chip assemblies.

2 Methodology

The noise and dark current of the Advanced Land Imager have been trended using dark current data collected as a part of daily Earth scene observations. During a typical data collection event or DCE, two seconds of dark current are collected before and after the Earth scene is imaged. These dark currents are used to establish baselines for all detectors for the corresponding observation and are also used to monitor the noise of the focal plane over time. For each DCE, the data from the second two-second dark period is used for the trending in this report[†].

The focal plane has been divided into several sections for this analysis, owing to the different noise and dark current produced by different detectors. For the noise analysis, the focal plane is divided by band and SCA. For the dark current analysis, odd and even detectors are treated separately for all bands. Results for the Panchromatic band have been additionally divided by tri-reads (each Panchromatic detector is read three times for each Multispectral detector read. Each tri-read results in a different dark current value for each detector.). Finally, SCA 4 for the SWIR bands has been divided into four sections to account for the enhanced dark current values observed near detector 1200.

For each data collection event, the noise has been calculated as the mean of individual detector noise values and the dark current has been calculated as the mean of individual detector dark current values.

Data collection event numbers, calendar dates and days since launch are provided as a reference in Table 1.

[†] All SWIR detectors have a transient effect associated with the initial data collected following the focal plane turn-on. Additionally, ground processing sometimes requires fill data to be added to the end of each data set. As a result, the first and last twenty-five frames from all data sets have been excluded from trending analysis.

Table 1: Data Collection Event Dates

Year	GMT Day	Day*	Data Collection Event Count
2000	330	5	1-3
	331	6	4
	336	11	5-6
	337	12	7-8
	338	13	9-10
	339	14	11-12
	340	15	13-14
	341	16	15-17
	342	17	18-20
	343	18	21
	344	19	22-23
	345	20	24-27
	346	21	28-29
	347	22	30-32
	348	23	33-36
	349	24	37-41
	350	25	42-44
	351	26	45-46
	352	27	47-51
	353	28	52-54
	354	29	55-59
	355	30	60-63
	356	31	64-66
	357	32	67-70
	358	33	7174
	359	34	75-79
	360	35	80-87
	361	36	88-92
	362	37	93-98
	363	38	99-103
	364	39	104-110
	365	40	111-116
	366	41	117-119
2001	001	42	120-123
	002	43	124-129
	003	44	130-137
	004	45	138-143
	005	46	144-150
	006	47	151-154
	007	48	155-159
	008	49	160-164
	009	50	165-168
	010	51	169-172
	011	52	173-178
	012	53	179-185
	013	54	186-192
	014	55	193-198
	015	56	199-203
	016	57	204-207
	017	58	208-213
	018	59	214-217
	019	60	218-224

*Since launch.

3 Noise Trending

The results of the ALI focal plane noise trending are provided in Figures 1-10 and Table 2. Each figure depicts the results of an individual band. Within each figure, the results for each sensor chip assembly are provided. Table 2 lists the mean and standard deviation of noise values, grouped by bands, in a similar fashion.

The mean noise value levels for all bands and SCAs is less than 1 digital number, except for the Panchromatic Band on SCA 3 (1.15 digital numbers) and Band 7 SCAs 1, 2, and 4 (1.06, 1.09, and 1.01 digital numbers, respectively). The standard deviation of detector noise is less than 0.05 digital numbers for all VNIR bands and SCAs. The repeatability of some SWIR SCAs is slightly higher with a maximum standard deviation of 0.099 digital numbers for Band 7, SCA 2.

The apparent systematic increase in detector noise across several spectral bands for some particular DCEs is the result of focal plane outgassing performed at the times of those observations. All ALI detectors were heated to 270 K five times during the first sixty days in orbit to drive-off contaminant build-up on the focal plane filter surfaces. This heating resulted in increased detector dark current and noise, particularly in the short wave infrared bands (5p, 5, 7). Outgassing periods correspond to DCE numbers 55, 140, 160, 190, and 219.

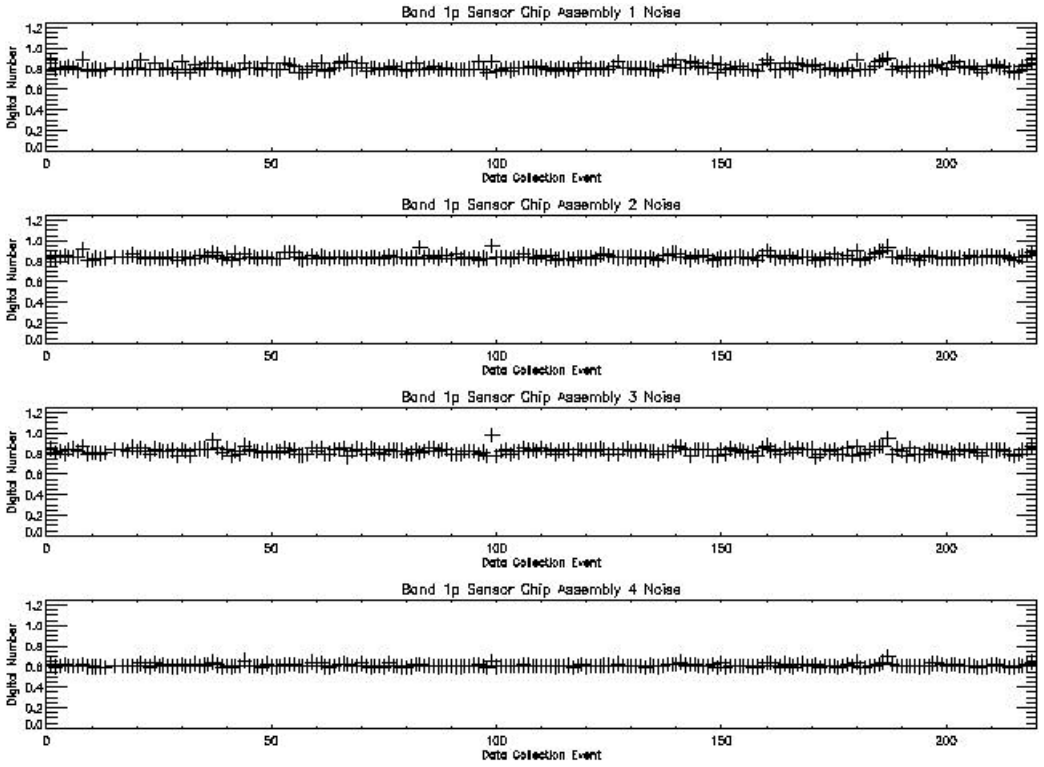

Figure 1: Noise trending for Band 1p. Detector outgassing occurred near DCE 55, 140, 160, 190, and 219.

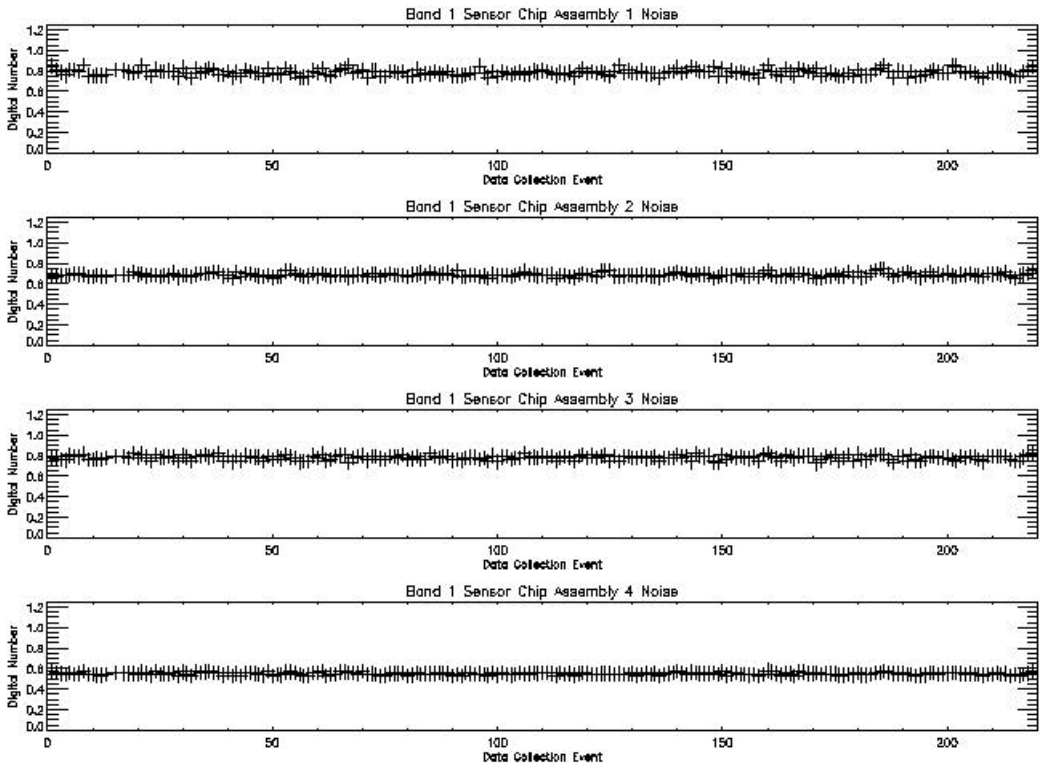

Figure 2: Noise trending for Band 1. Detector outgassing occurred near DCE 55, 140, 160, 190, and 219.

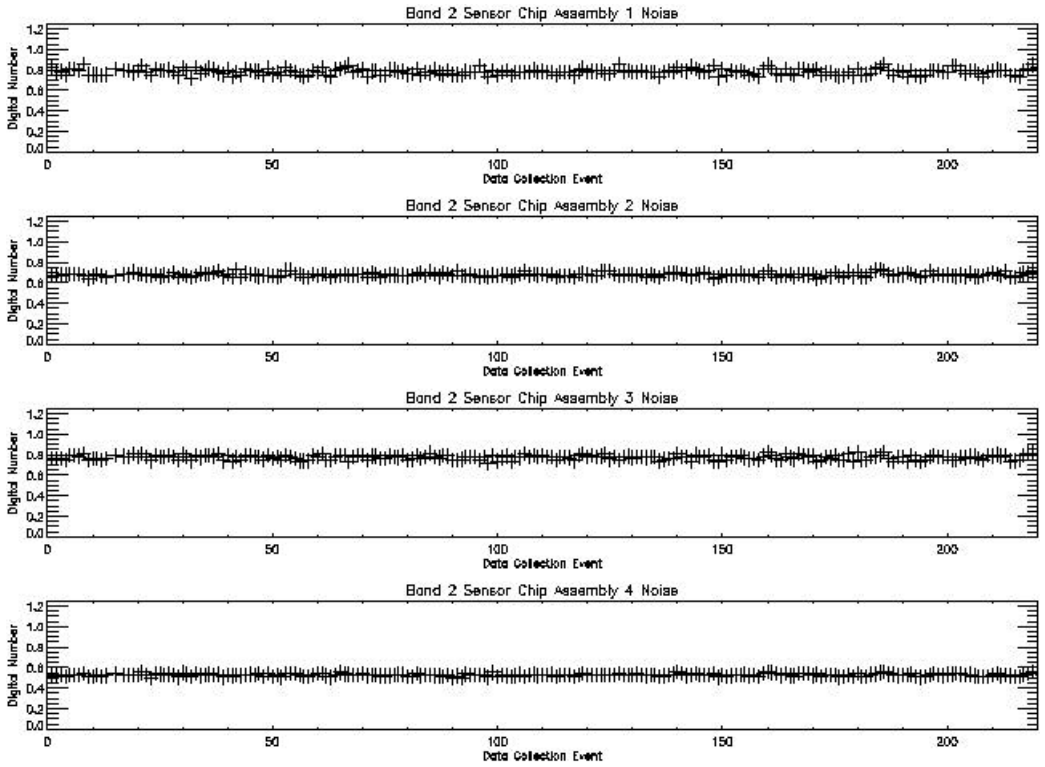

Figure 3: Noise trending for Band 2. Detector outgassing occurred near DCE 55, 140, 160, 190, and 219.

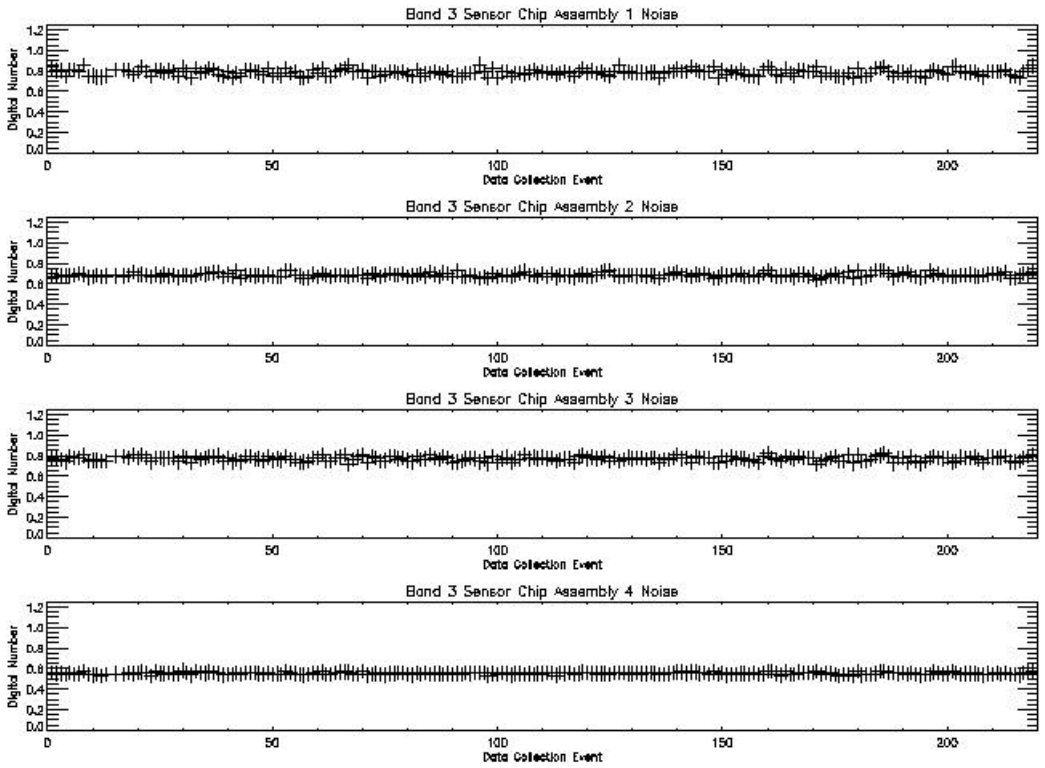

Figure 4: Noise trending for Band 3. Detector outgassing occurred near DCE 55, 140, 160, 190, and 219.

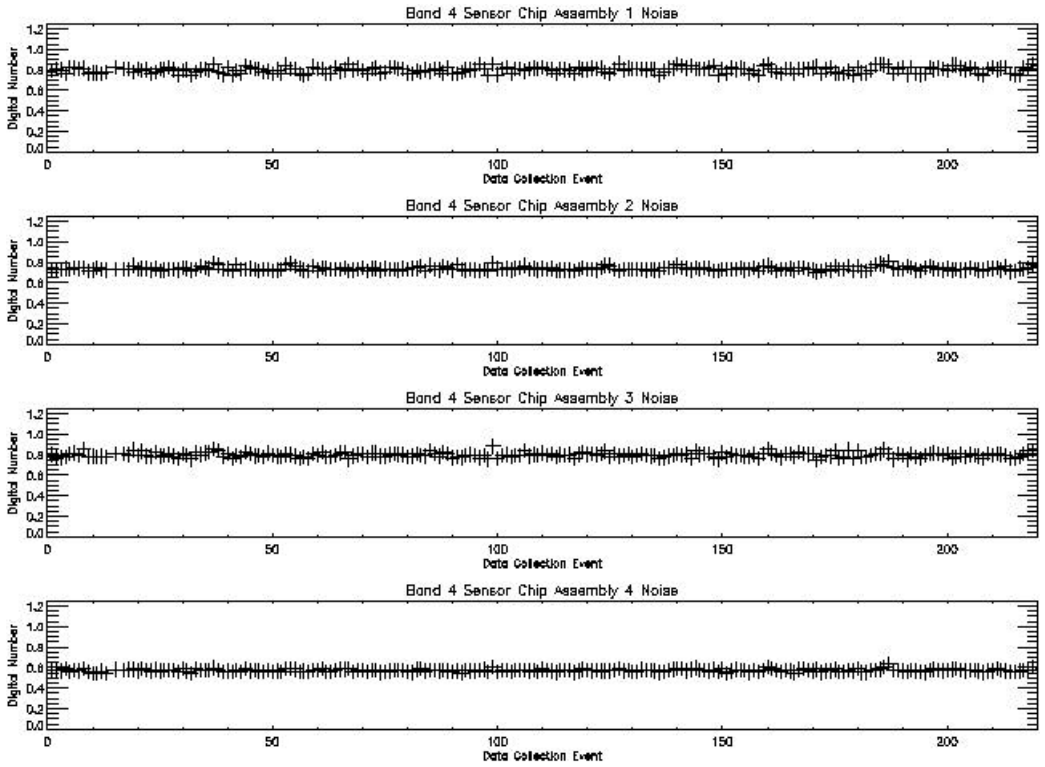

Figure 5: Noise trending for Band 4. Detector outgassing occurred near DCE 55, 140, 160, 190, and 219.

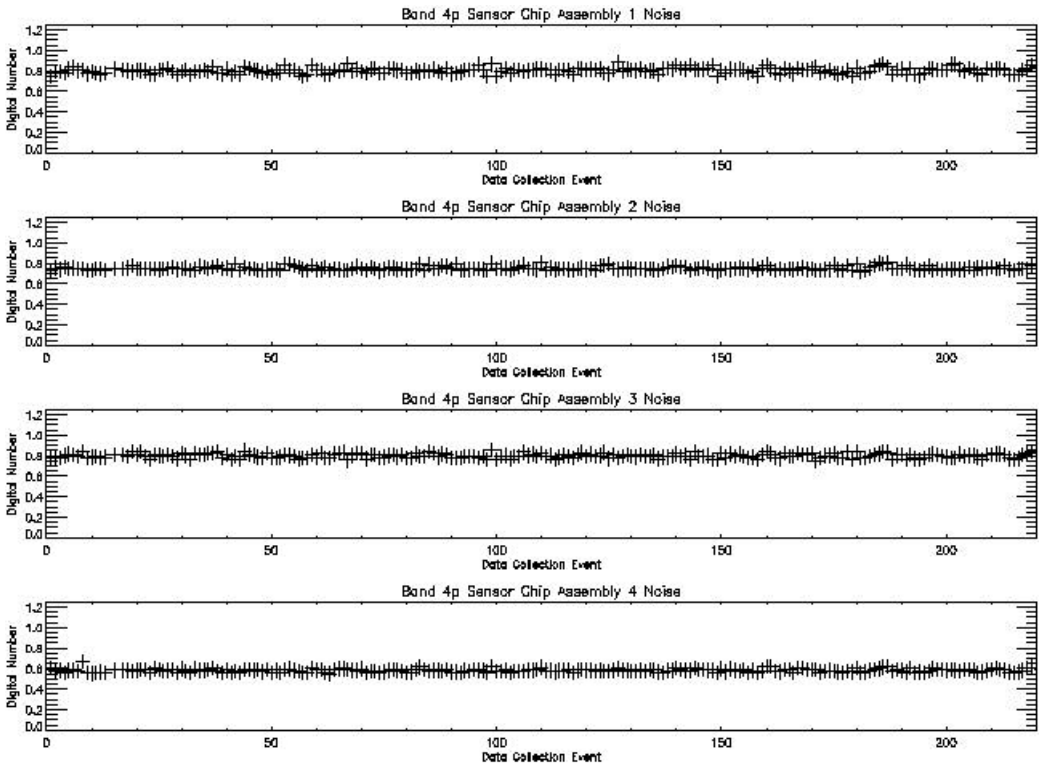

Figure 6: Noise trending for Band 4p. Detector outgassing occurred near DCE 55, 140, 160, 190, and 219.

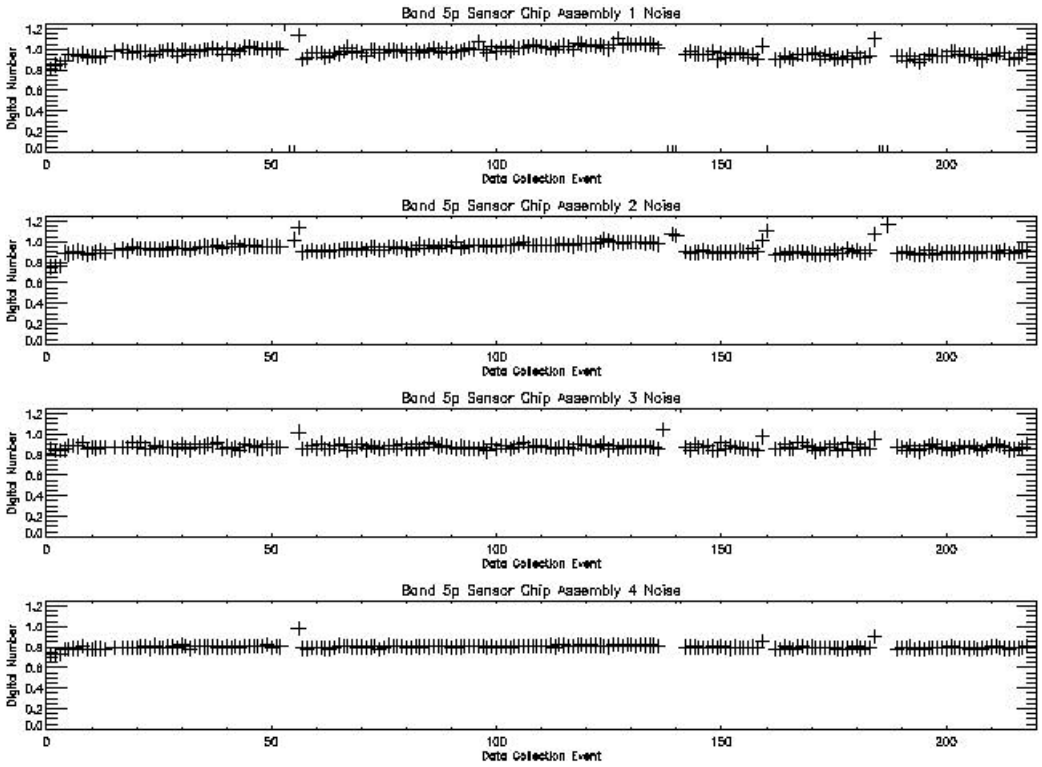

Figure 7: Noise trending for Band 5p. Detector outgassing occurred near DCE 55, 140, 160, 190, and 219.

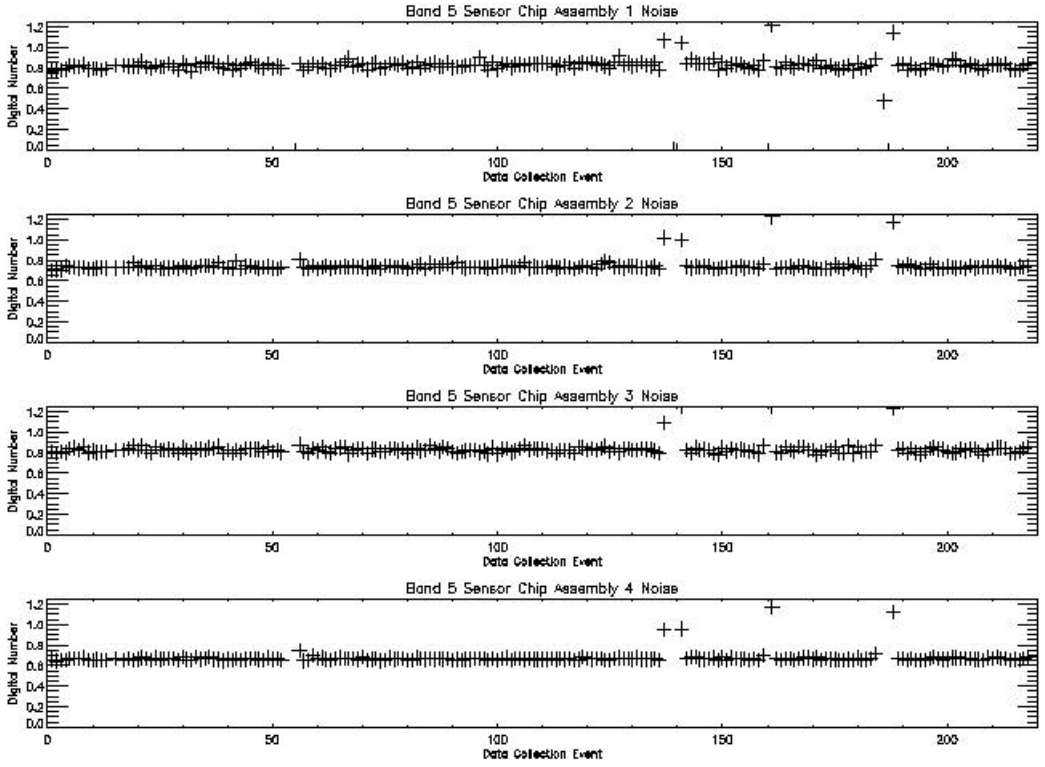

Figure 8: Noise trending for Band 5. Detector outgassing occurred near DCE 55, 140, 160, 190, and 219.

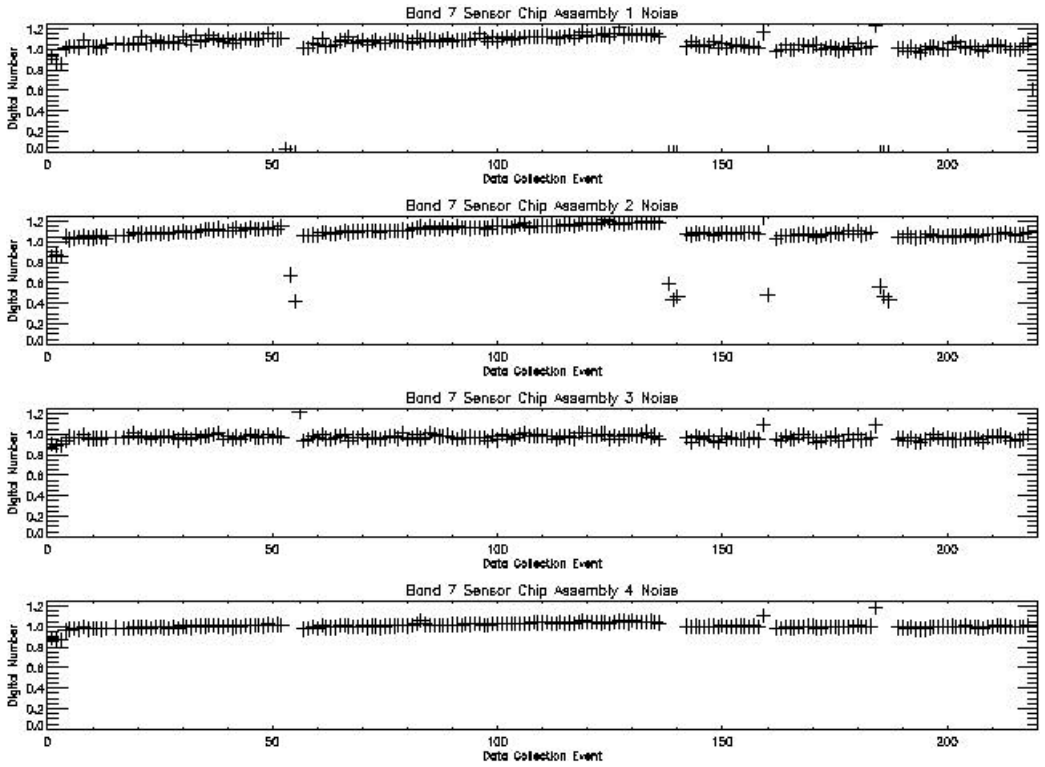

Figure 9: Noise trending for Band 7. Detector outgassing occurred near DCE 55, 140, 160, 190, and 219.

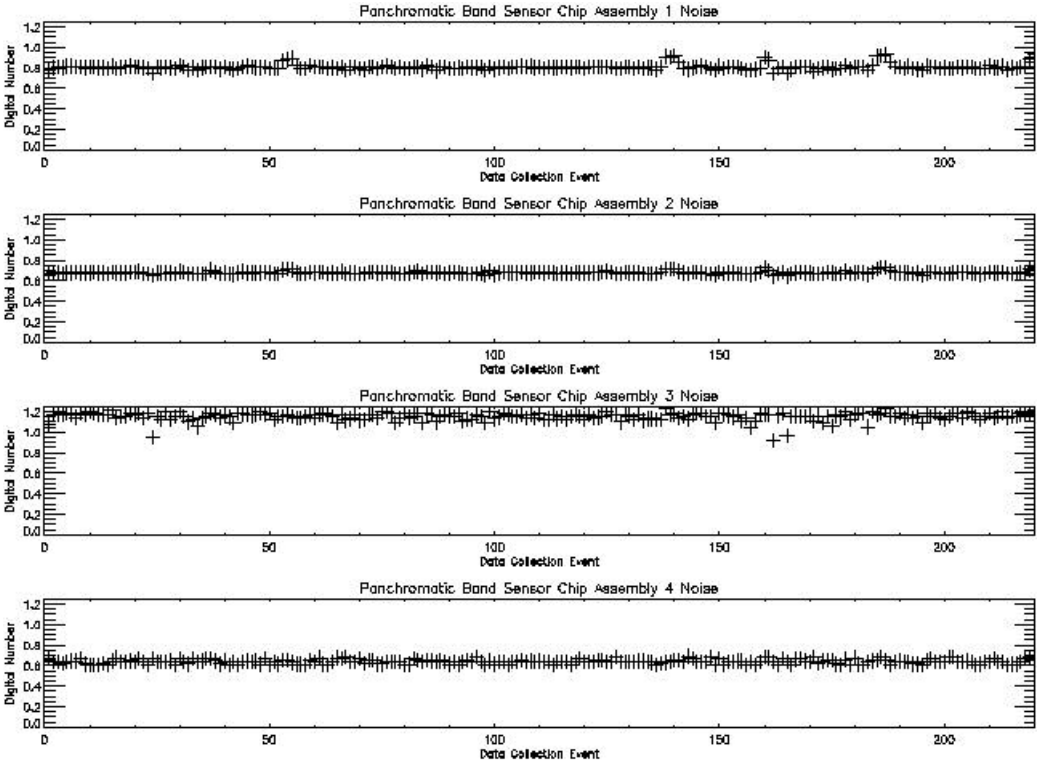

Figure 10: Noise trending for the Panchromatic Band. Detector outgassing occurred near DCE 55, 140, 160, 190, and 219.

Table 2: Noise Trending Statistics

Band	SCA	Preflight Mean (Digital Number)	Flight Mean (Digital Number)	Flight Std. Deviation (Digital Number)
1p	1	0.88	0.81	0.030
1p	2	0.86	0.84	0.022
1p	3	0.91	0.83	0.028
1p	4	0.60	0.61	0.014
1	1	0.83	0.78	0.029
1	2	0.73	0.69	0.017
1	3	0.87	0.78	0.021
1	4	0.54	0.55	0.012
2	1	0.82	0.78	0.028
2	2	0.70	0.68	0.017
2	3	0.84	0.77	0.022
2	4	0.53	0.53	0.012
3	1	0.83	0.78	0.030
3	2	0.72	0.69	0.018
3	3	0.85	0.77	0.022
3	4	0.55	0.55	0.010
4	1	0.86	0.80	0.029
4	2	0.77	0.74	0.019
4	3	0.88	0.80	0.022
4	4	0.57	0.57	0.013
4p	1	0.85	0.80	0.027
4p	2	0.78	0.75	0.018
4p	3	0.87	0.80	0.022
4p	4	0.58	0.58	0.016
5p	1	0.92	0.97	0.042
5p	2	0.83	0.94	0.031
5p	3	0.92	0.88	0.021
5p	4	0.75	0.81	0.025
5	1	0.87	0.83	0.035
5	2	0.75	0.74	0.035
5	3	0.89	0.83	0.037
5	4	0.67	0.70	0.024
7	1	0.99	1.06	0.068
7	2	0.90	1.09	0.099
7	3	0.98	0.97	0.031
7	4	0.90	1.01	0.037
Pan	1	0.80	0.81	0.029
Pan	2	0.67	0.68	0.013
Pan	3	1.05	1.15	0.039
Pan	4	0.64	0.64	0.021

4 Dark Current Trending

The results of the ALI focal plane dark current trending for Bands 1p, 1, 2, 3, 4, 4p are provided in Figures 11-22. Each figure depicts the results of an individual band. Within each figure, the results of odd and even detectors for each sensor chip assembly are provided. The results of dark current trending for Bands 5p, 5, and 7 are provided in Figures 23-28. Each figure depicts the results of an individual band. Within each figure, the results of odd and even detectors for each sensor chip assembly are provided. SCA 4 is further divided into four quadrants, owing to the rapid change in dark current near the previously identified 'hot spot' near detector 1200[6]. Finally, the results of dark current trending for the Panchromatic Band are provided in Figures 29-34. Each figure depicts the results of an individual tri-read. Within each figure, the results of odd and even detectors for each sensor chip assembly are provided.

Table 3 lists the mean and standard deviation of dark current values, grouped by bands, in a similar fashion.

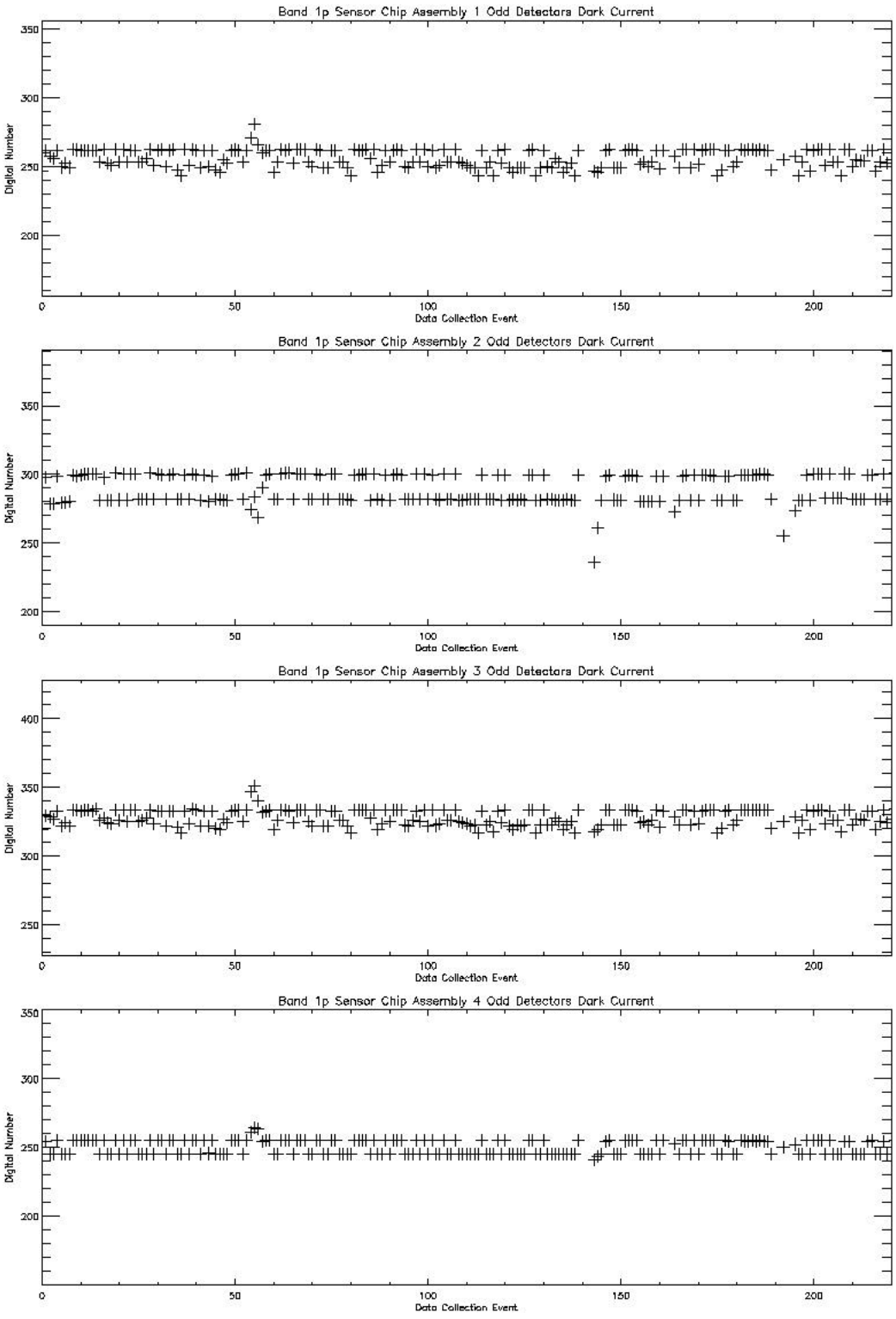

Figure 11: Dark current trending for Band 1p odd detectors. Detector outgassing occurred near DCE 55, 140, 160, 190, and 219.

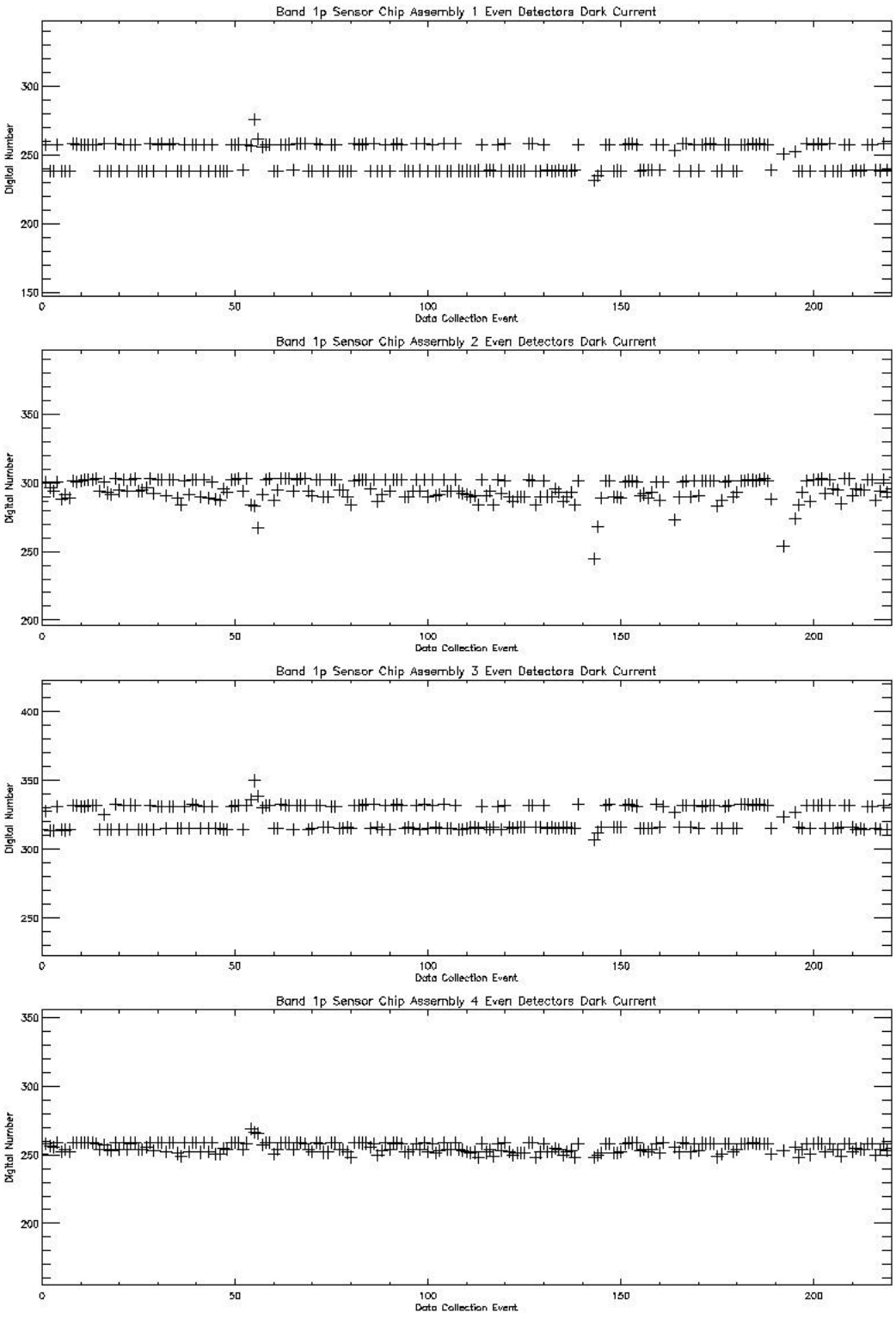

Figure 12: Dark current trending for Band 1p even detectors. Detector outgassing occurred near DCE 55, 140, 160, 190, and 219.

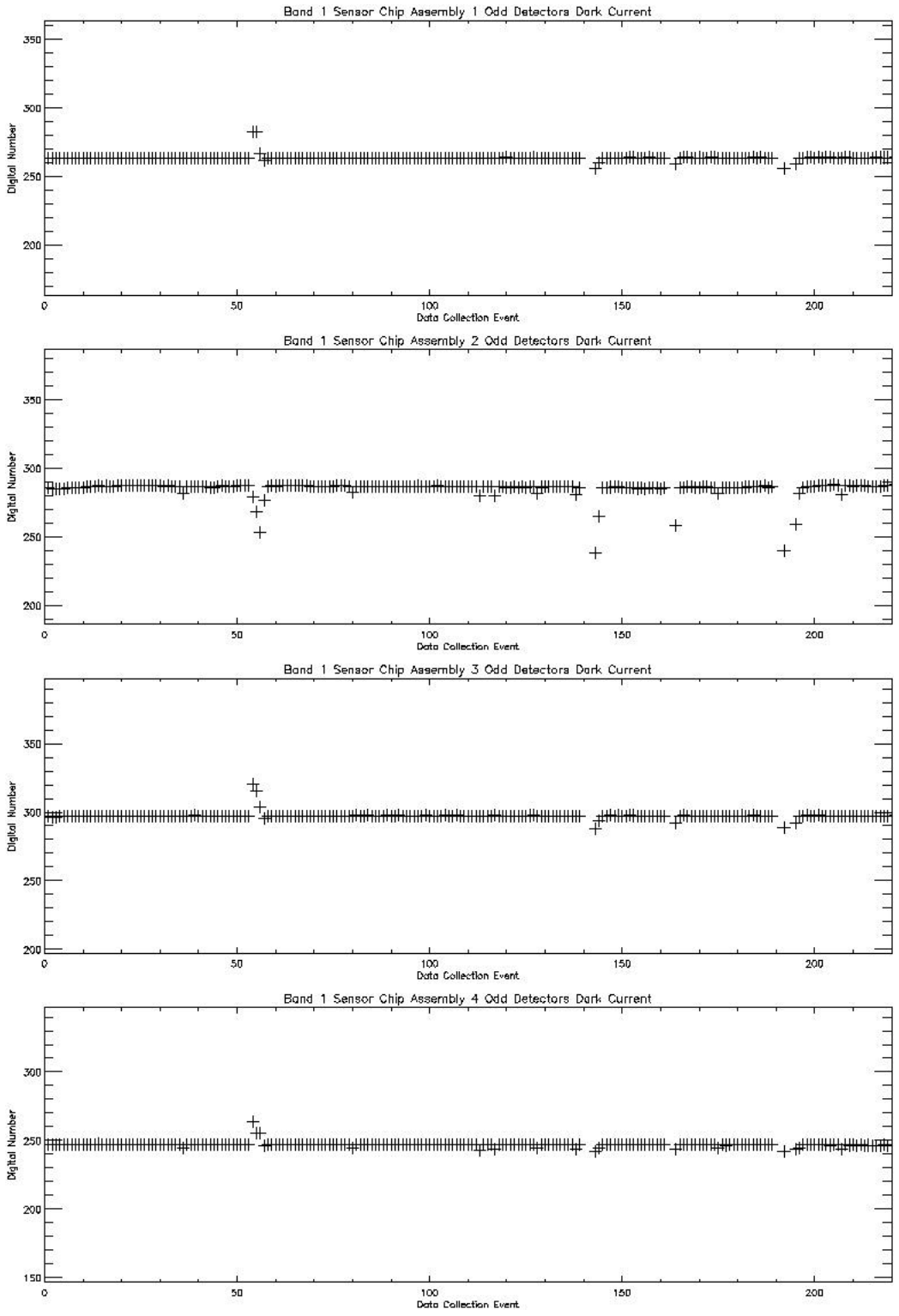

Figure 13: Dark current trending for Band 1 odd detectors. Detector outgassing occurred near DCE 55, 140, 160, 190, and 219.

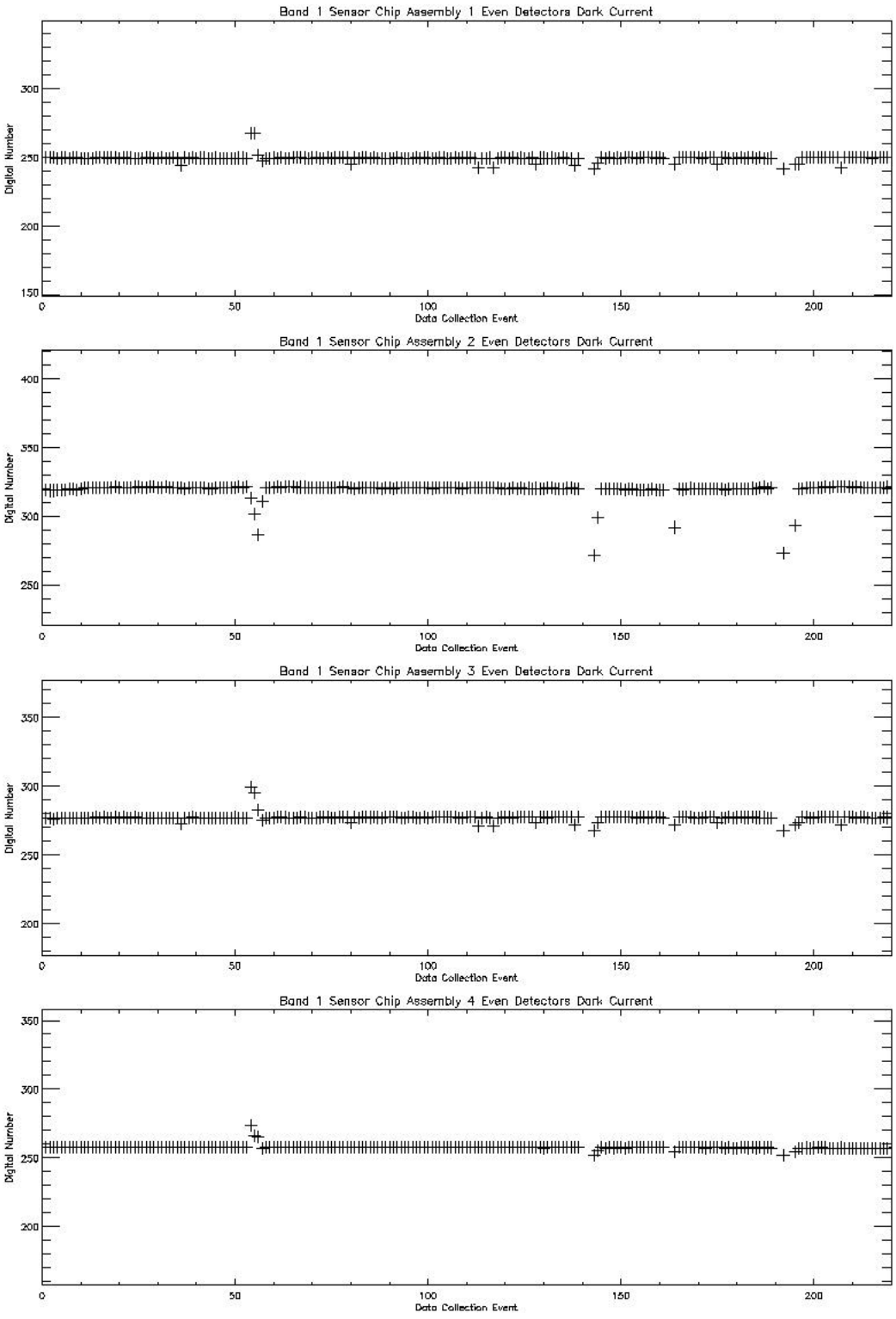

Figure 14: Dark current trending for Band 1 even detectors. Detector outgassing occurred near DCE 55, 140, 160, 190, and 219.

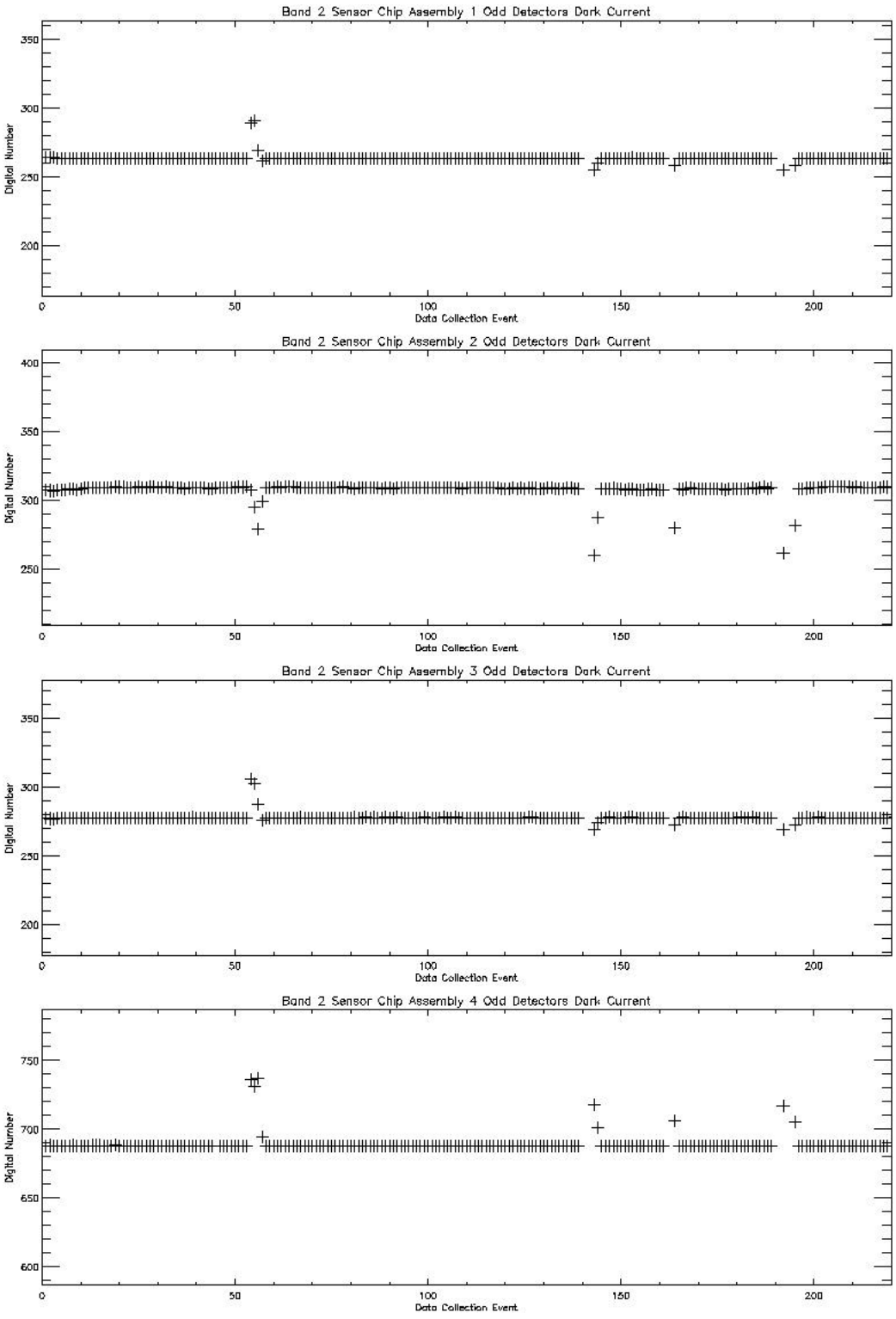

Figure 15: Dark current trending for Band 2 odd detectors. Detector outgassing occurred near DCE 55, 140, 160, 190, and 219.

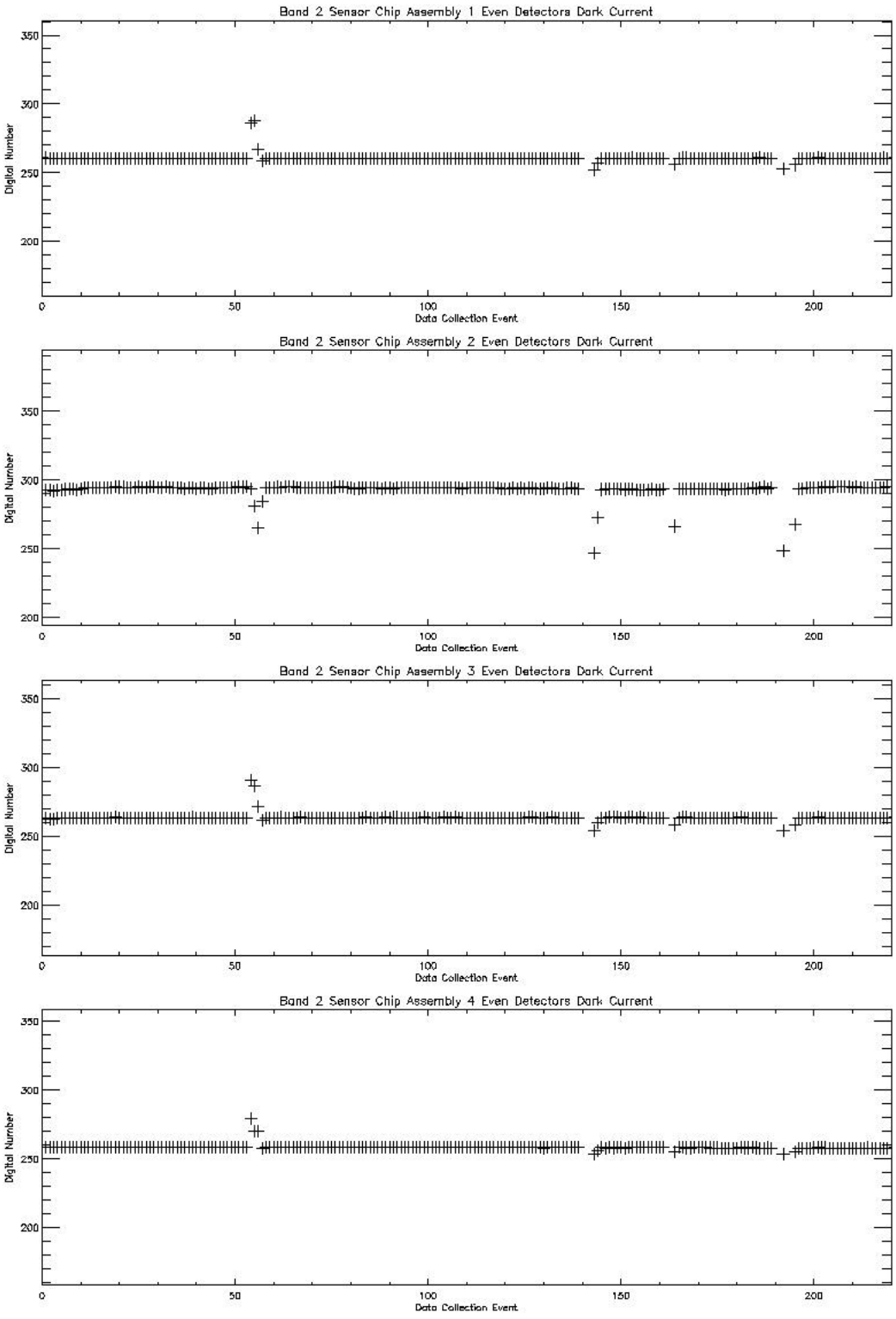

Figure 16: Dark current trending for Band 2 even detectors. Detector outgassing occurred near DCE 55, 140, 160, 190, and 219.

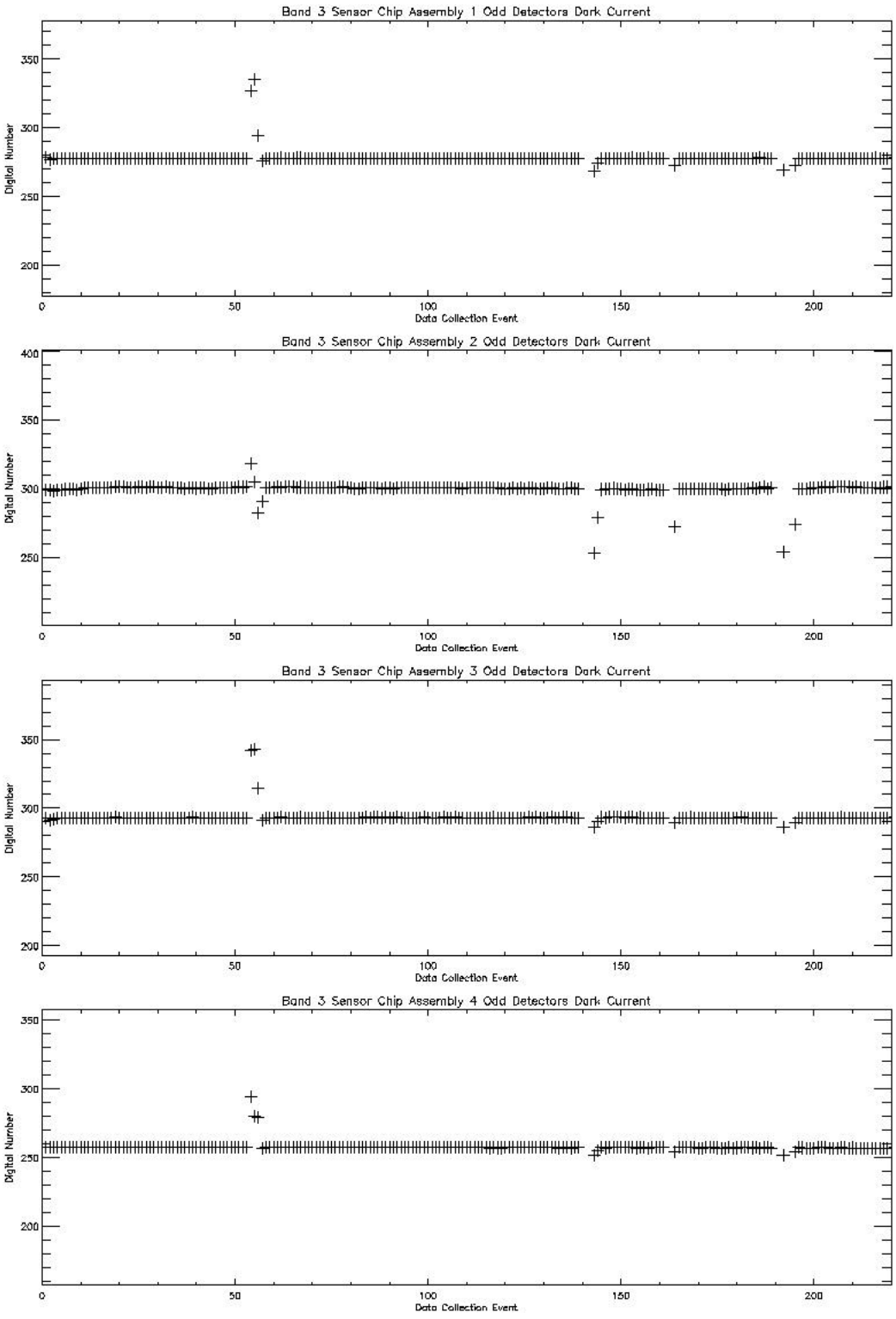

Figure 17: Dark current trending for Band 3 odd detectors. Detector outgassing occurred near DCE 55, 140, 160, 190, and 219.

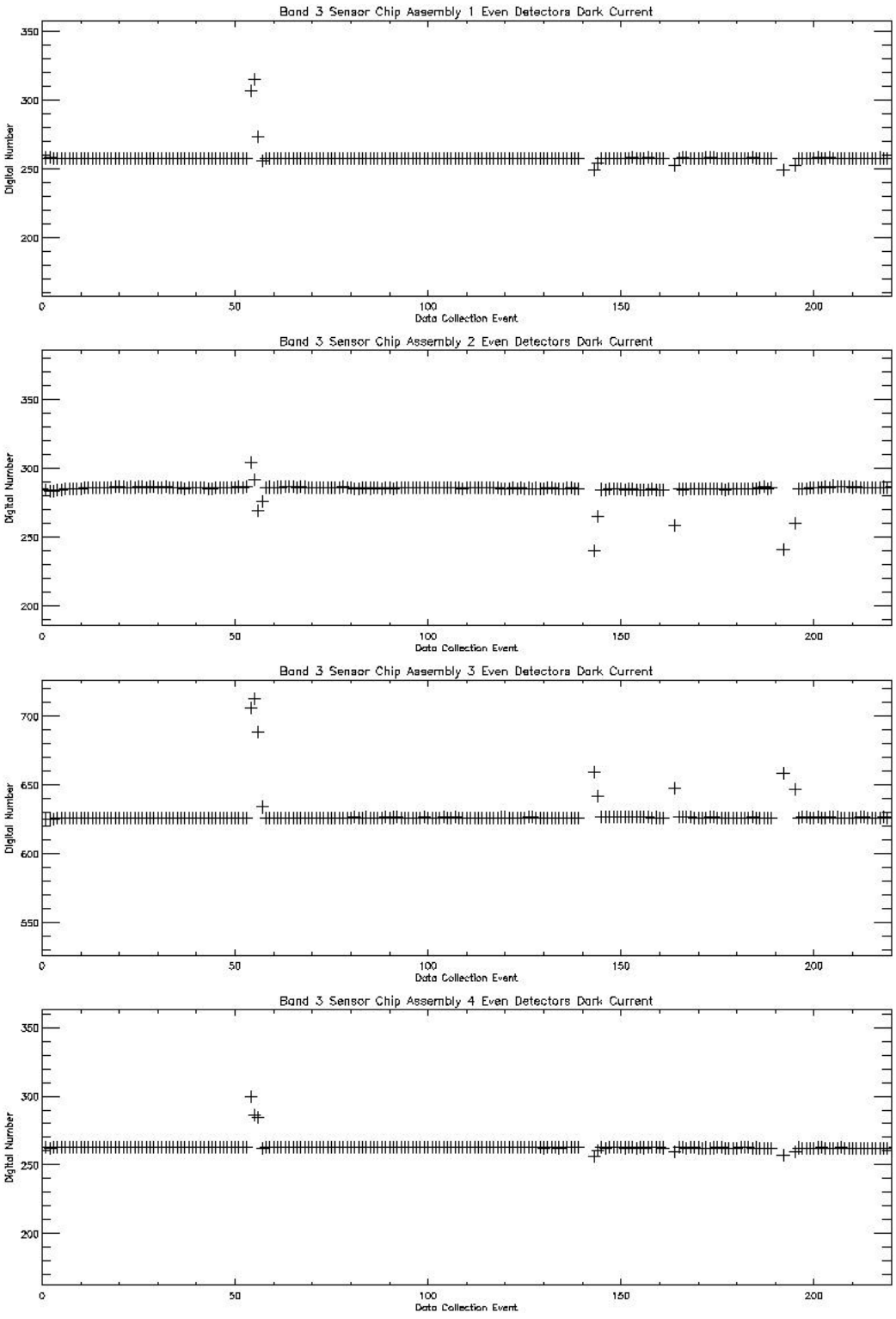

Figure 18: Dark current trending for Band 3 even detectors. Detector outgassing occurred near DCE 55, 140, 160, 190, and 219.

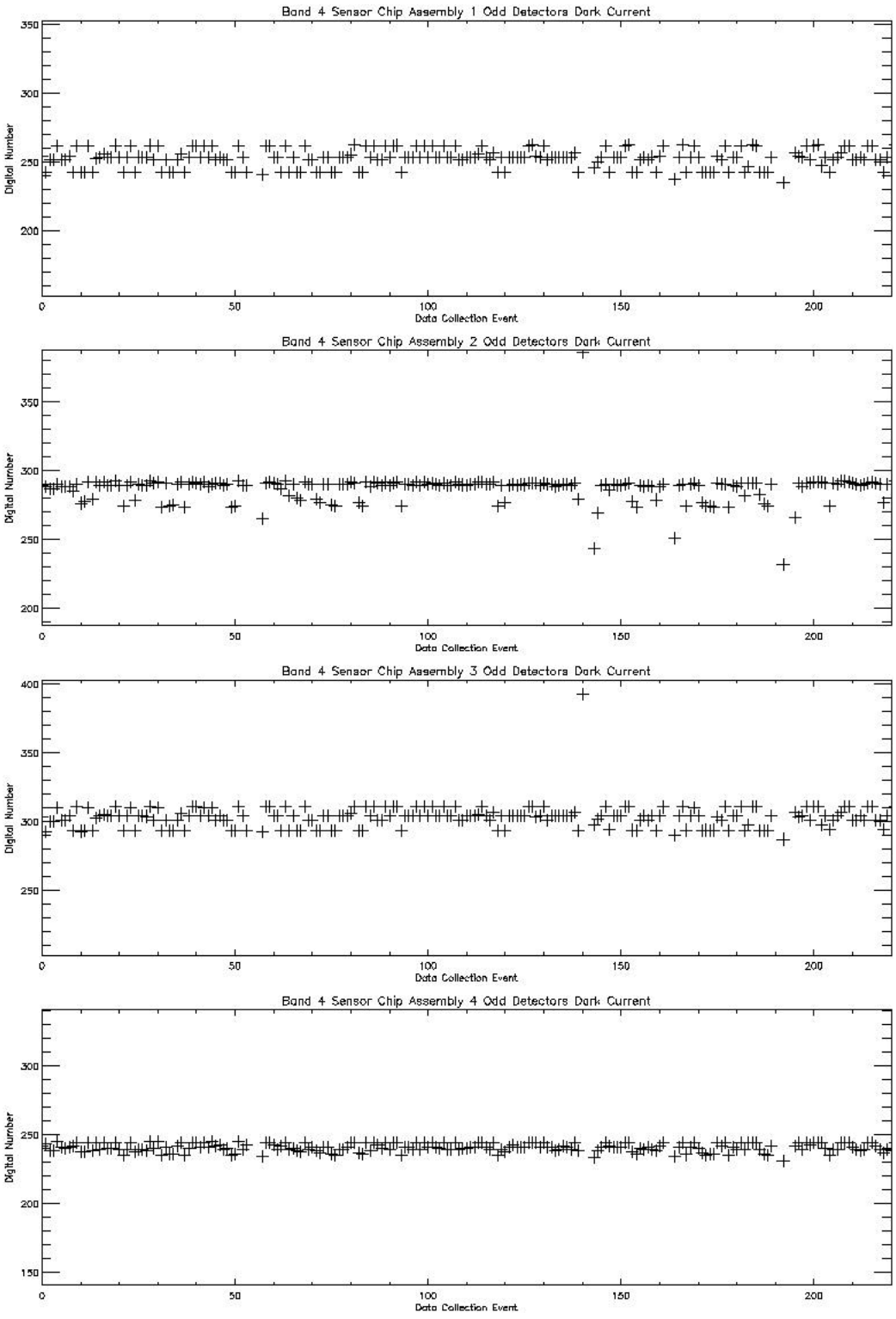

Figure 19: Dark current trending for Band 4 odd detectors. Detector outgassing occurred near DCE 55, 140, 160, 190, and 219.

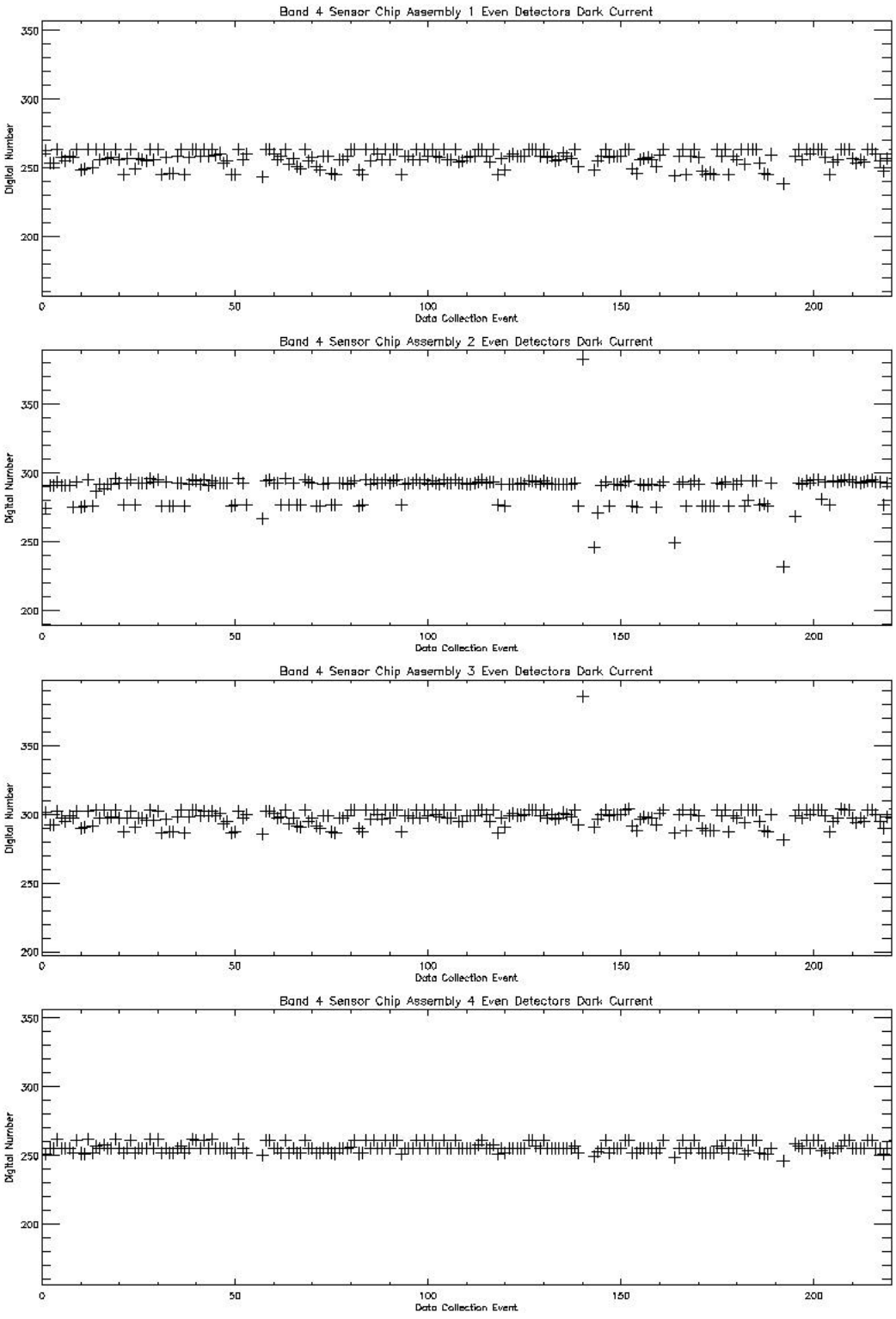

Figure 20: Dark current trending for Band 4 even detectors. Detector outgassing occurred near DCE 55, 140, 160, 190, and 219.

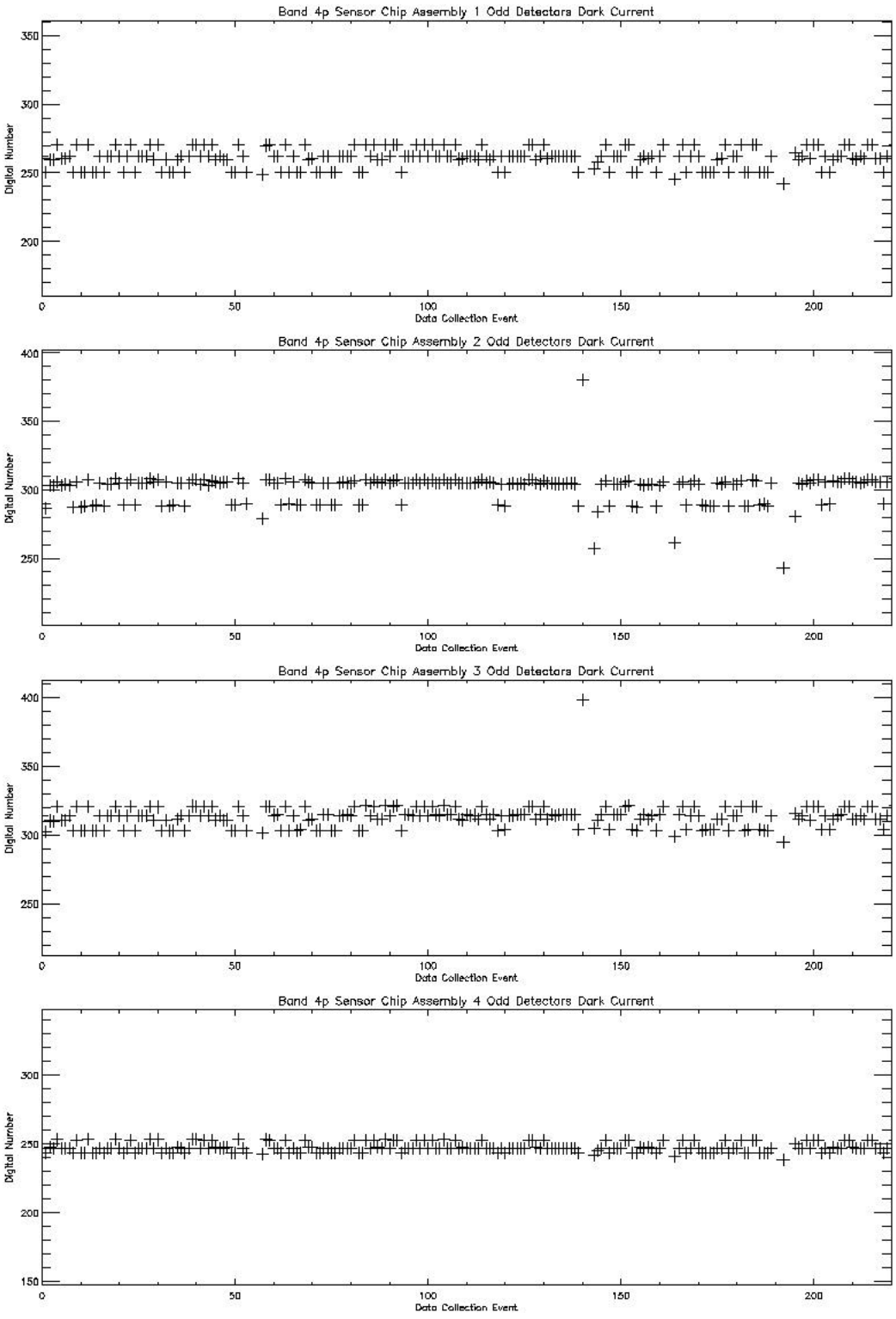

Figure 21: Dark current trending for Band 4p odd detectors. Detector outgassing occurred near DCE 55, 140, 160, 190, and 219.

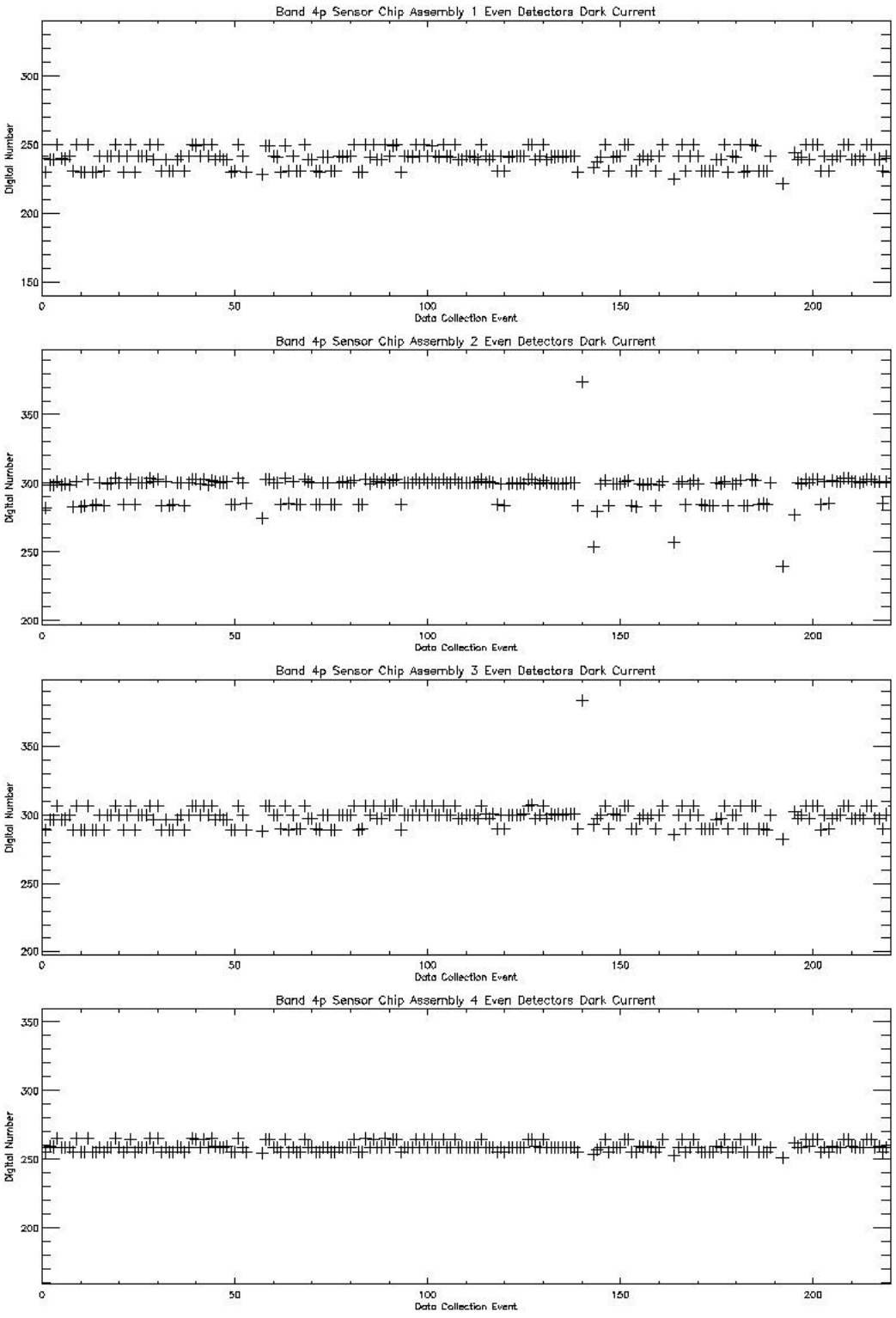

Figure 22: Dark current trending for Band 4p even detectors. Detector outgassing occurred near DCE 55, 140, 160, 190, and 219.

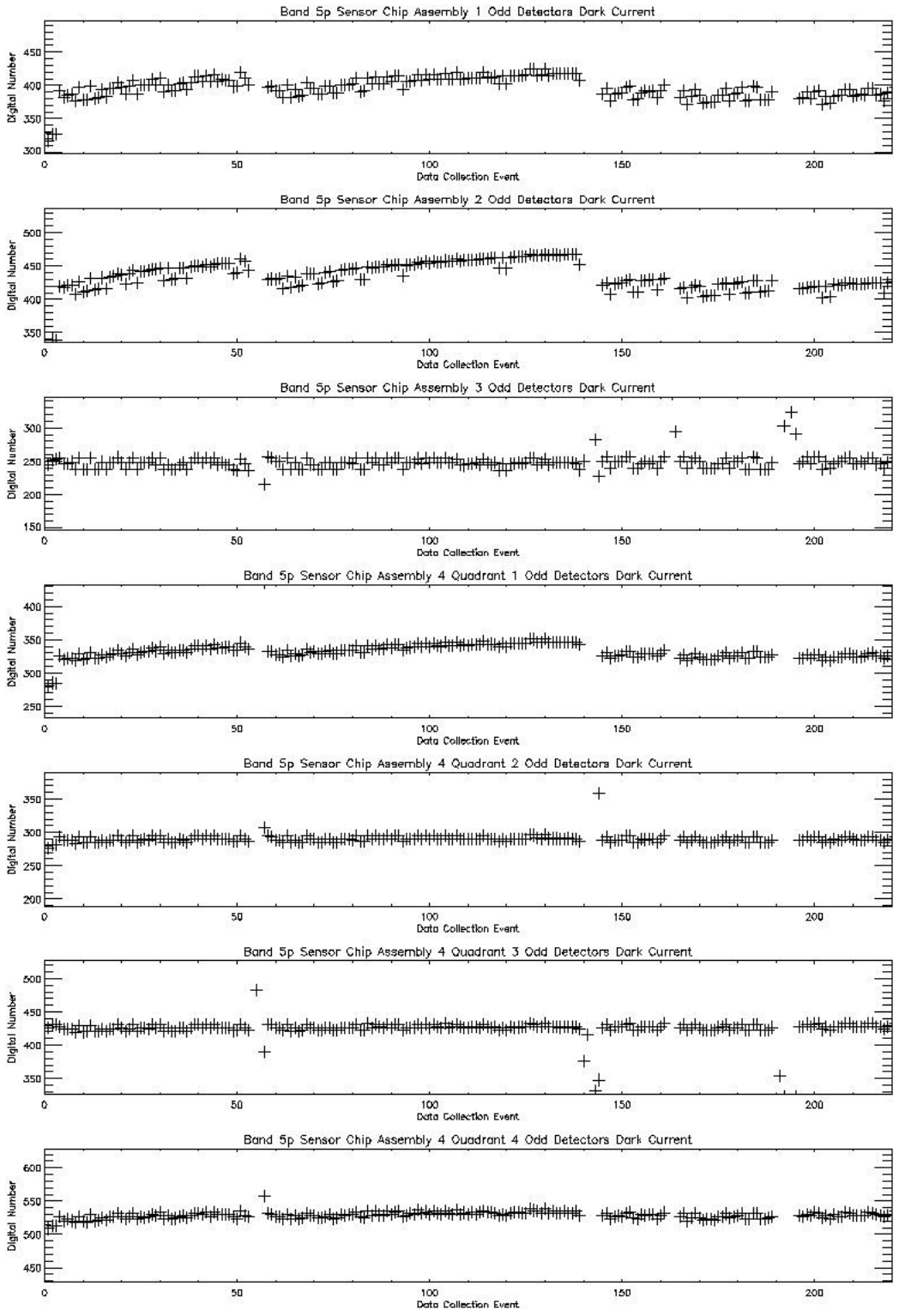

Figure 23: Dark current trending for Band 5p odd detectors. Detector outgassing occurred near DCE 55, 140, 160, 190, and 219.

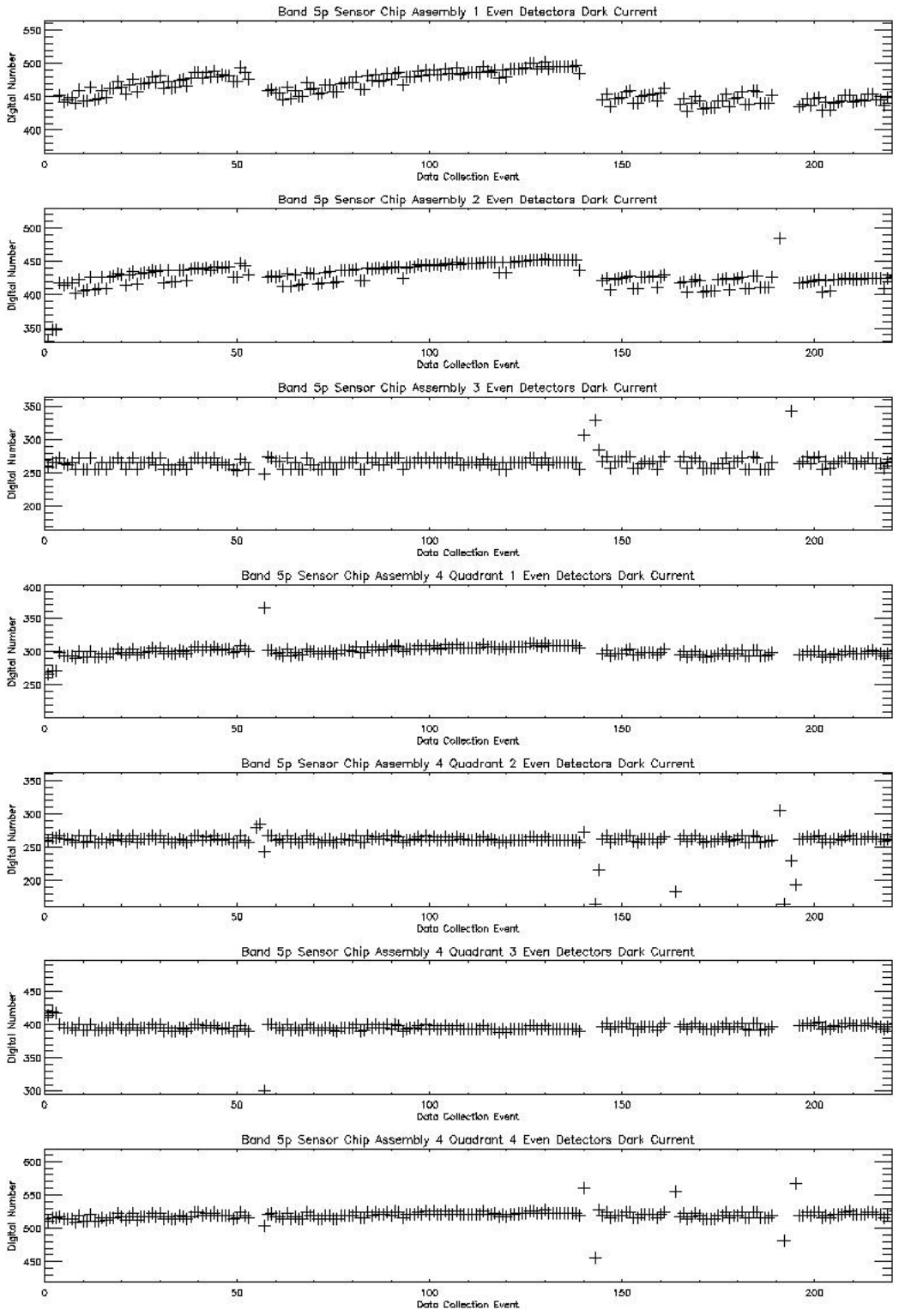

Figure 24: Dark current trending for Band 5p even detectors. Detector outgassing occurred near DCE 55, 140, 160, 190, and 219.

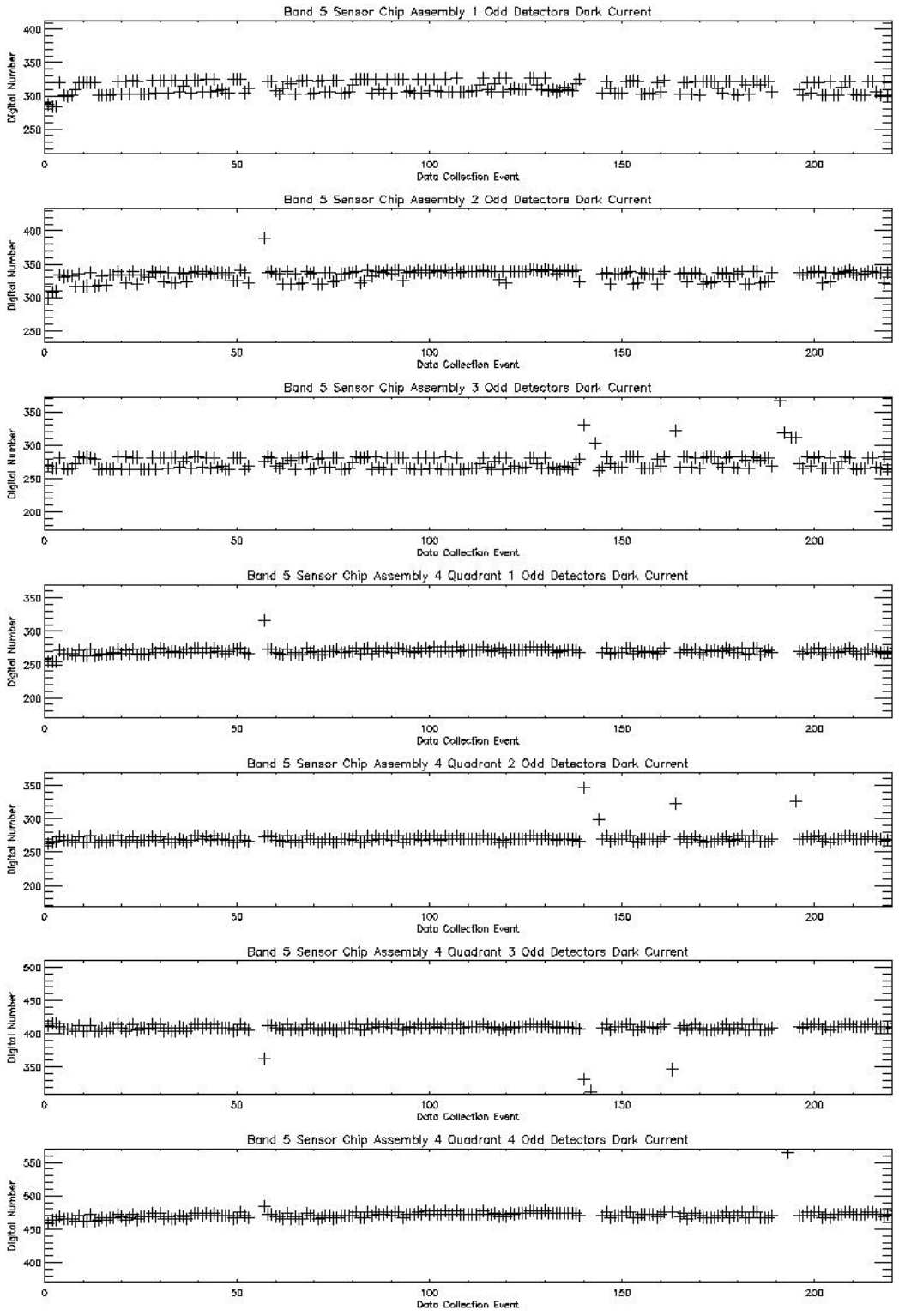

Figure 25: Dark current trending for Band 5 odd detectors. Detector outgassing occurred near DCE 55, 140, 160, 190, and 219.

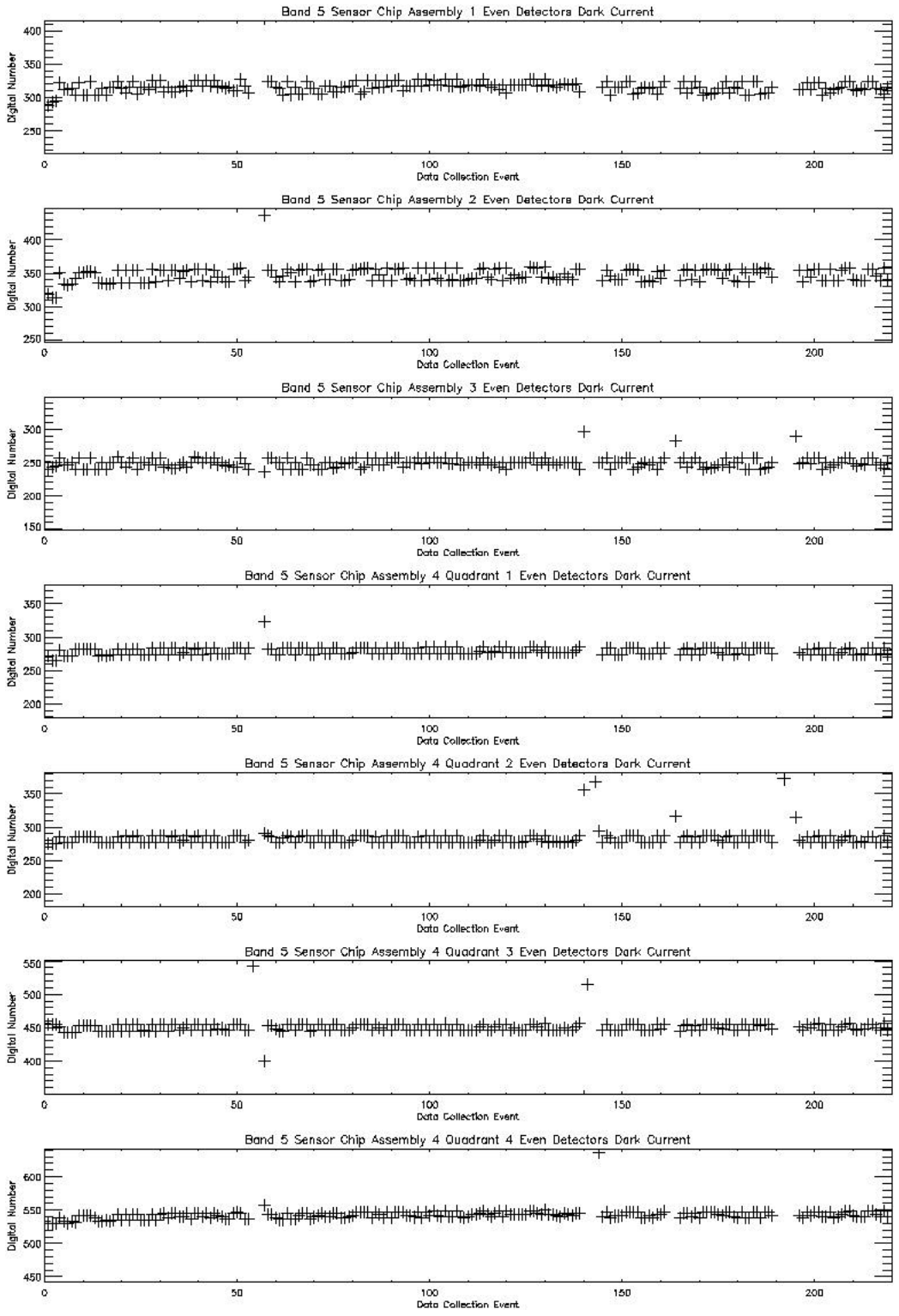

Figure 26: Dark current trending for Band 5 even detectors. Detector outgassing occurred near DCE 55, 140, 160, 190, and 219.

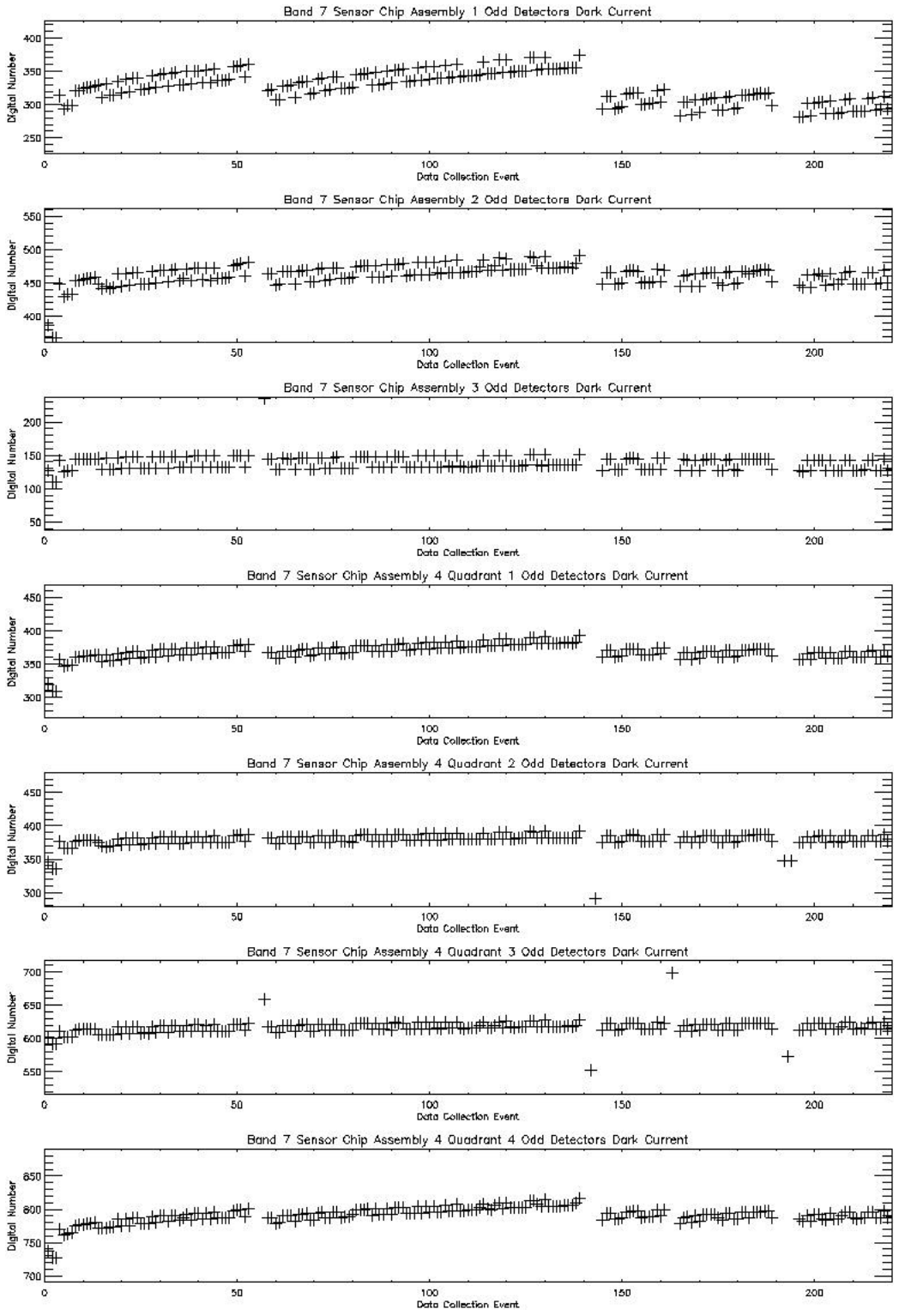

Figure 27: Dark current trending for Band 7 odd detectors. Detector outgassing occurred near DCE 55, 140, 160, 190, and 219.

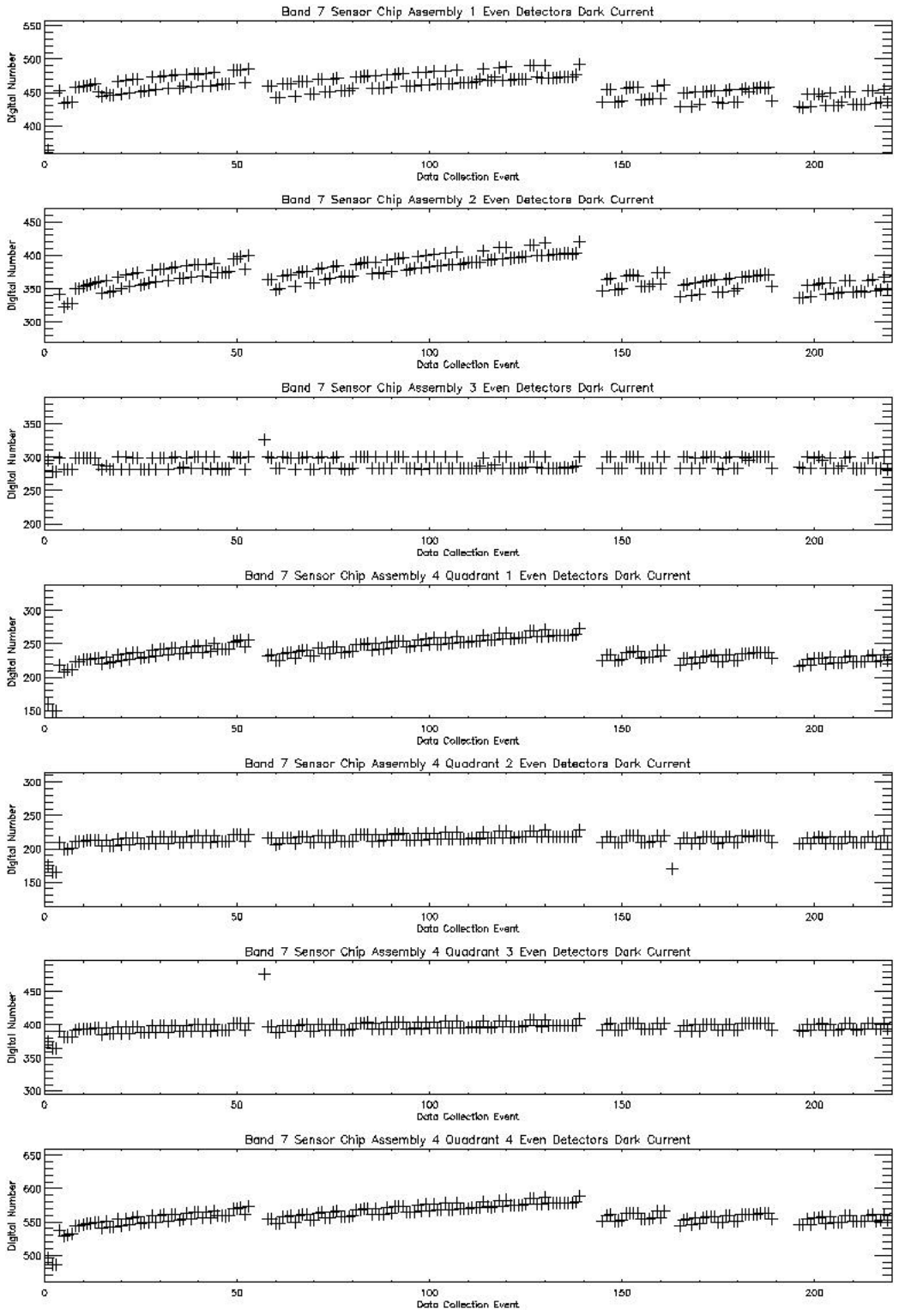

Figure 28: Dark current trending for Band 7 even detectors. Detector outgassing occurred near DCE 55, 140, 160, 190, and 219.

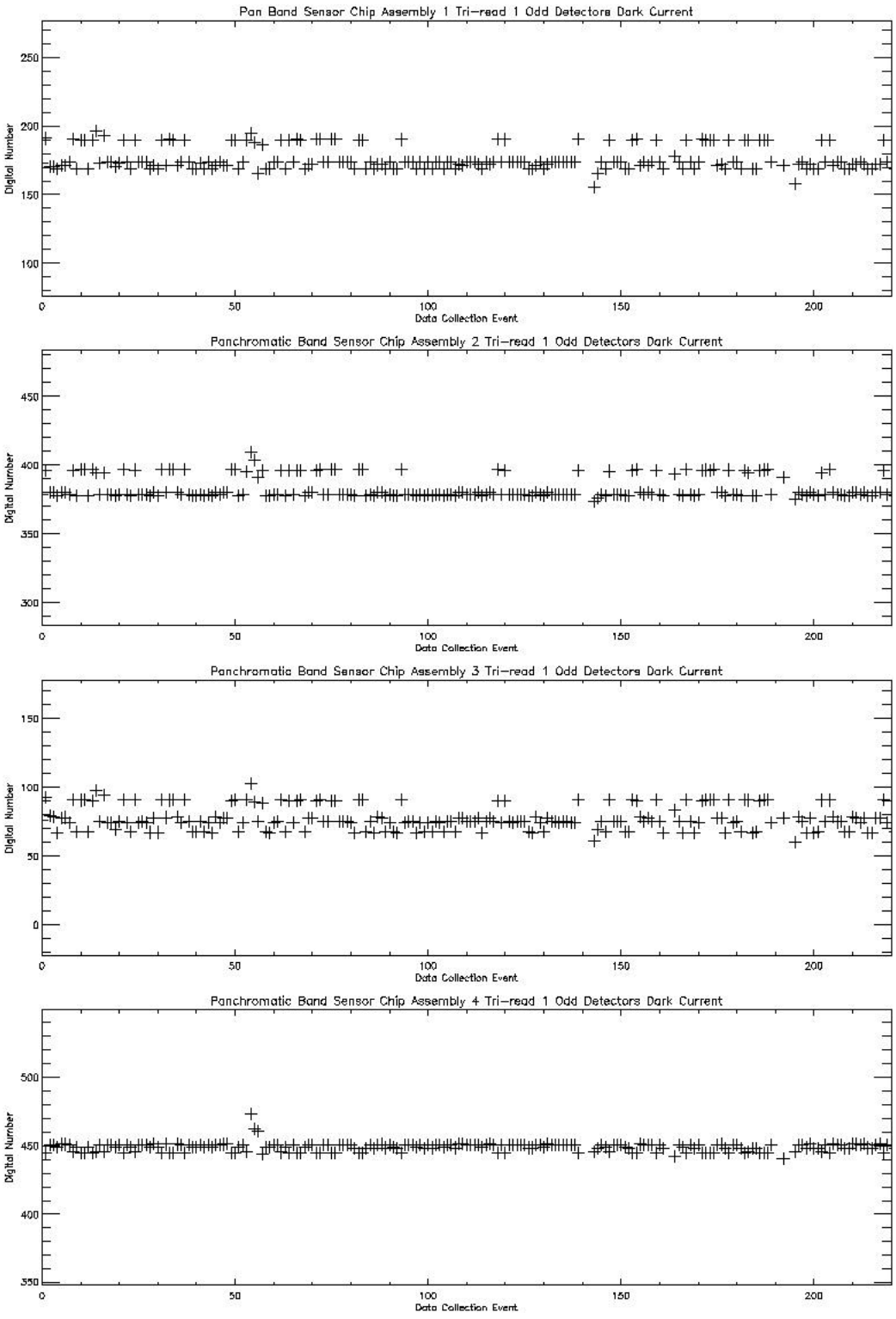

Figure 29: Dark current trending for Panchromatic Band tri-read #1 odd detectors. Detector outgassing occurred near DCE 55, 140, 160, 190, and 219.

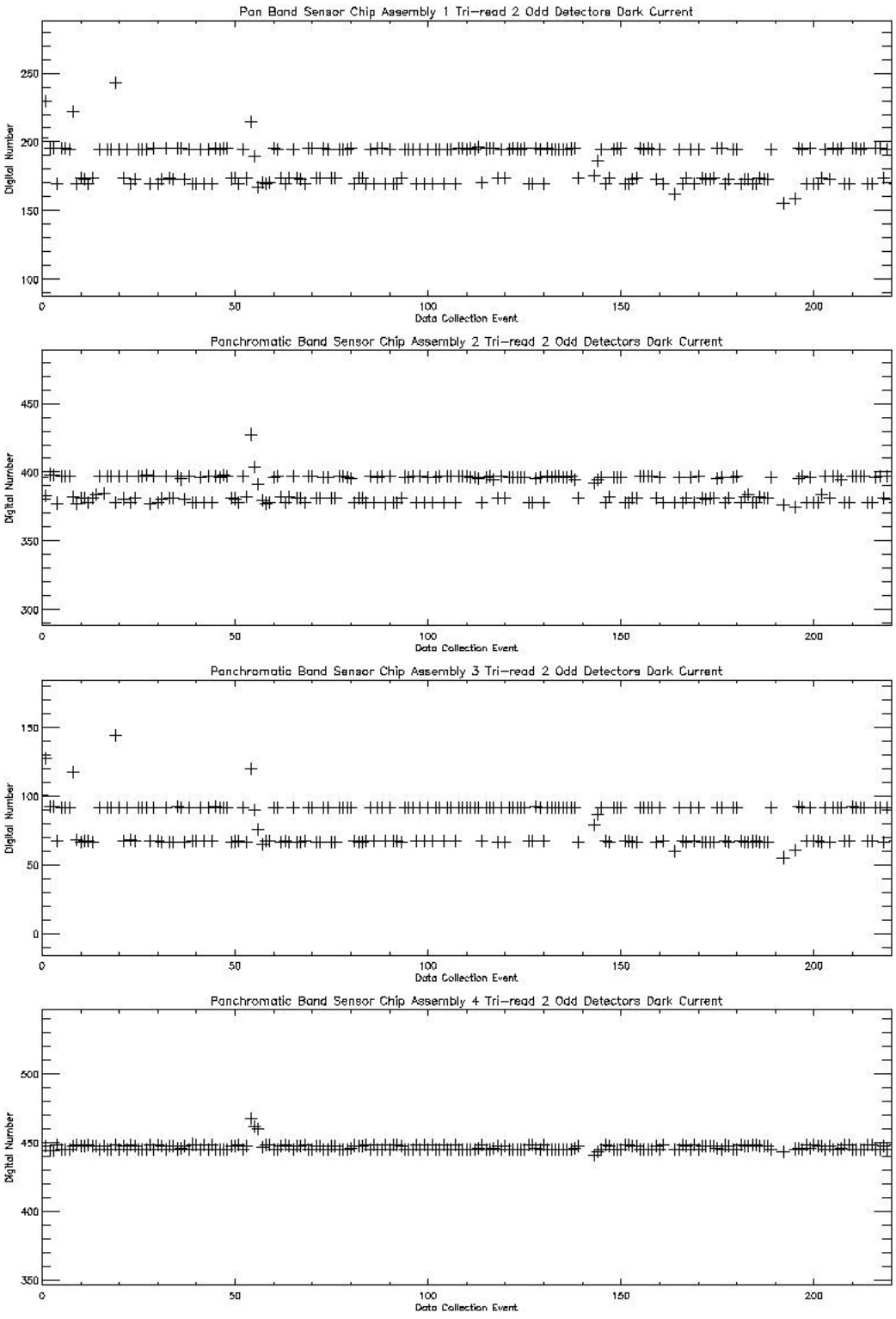

Figure 30: Dark current trending for Panchromatic Band tri-read #2 odd detectors. Detector outgassing occurred near DCE 55, 140, 160, 190, and 219.

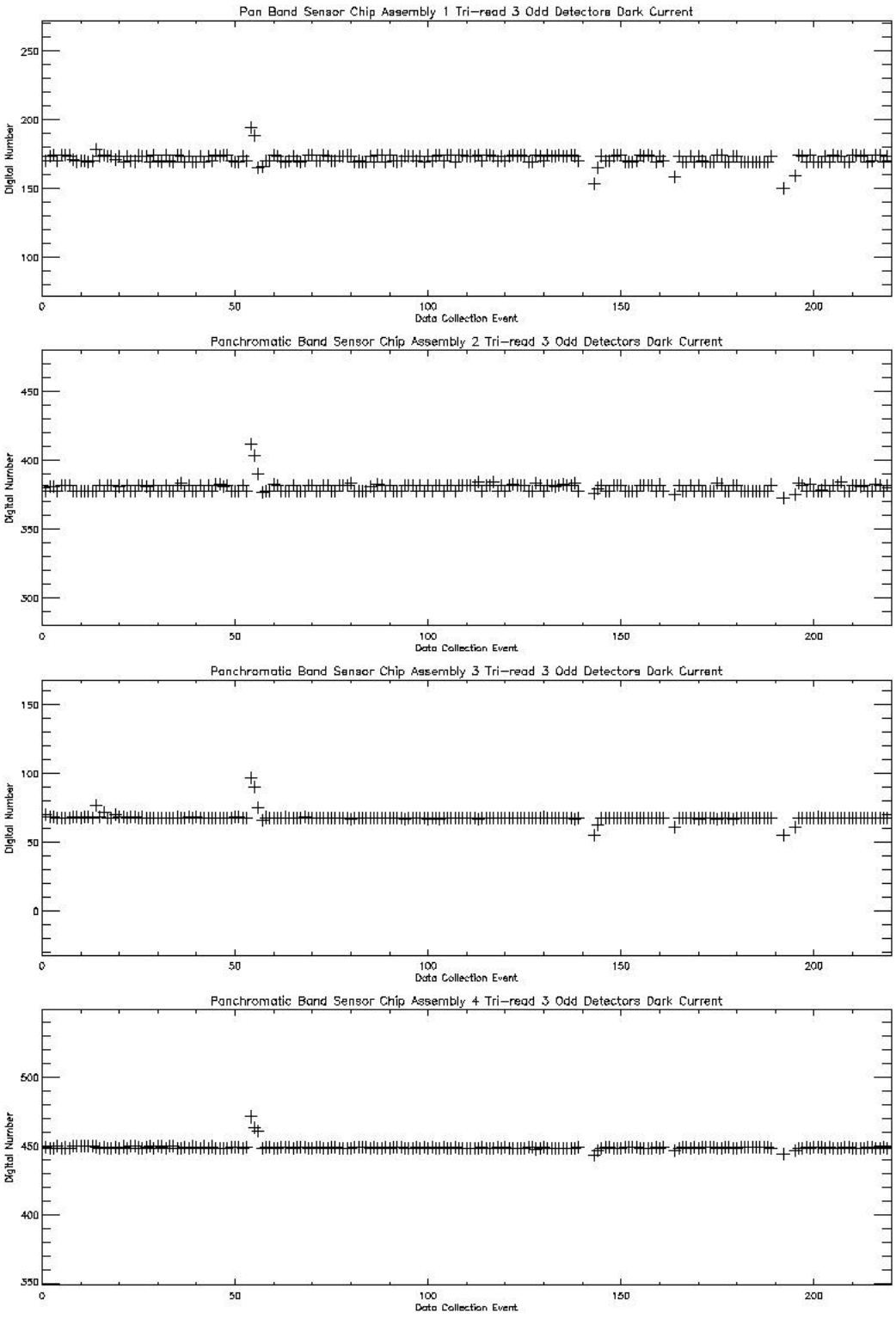

Figure 31: Dark current trending for Panchromatic Band tri-read #3 odd detectors. Detector outgassing occurred near DCE 55, 140, 160, 190, and 219.

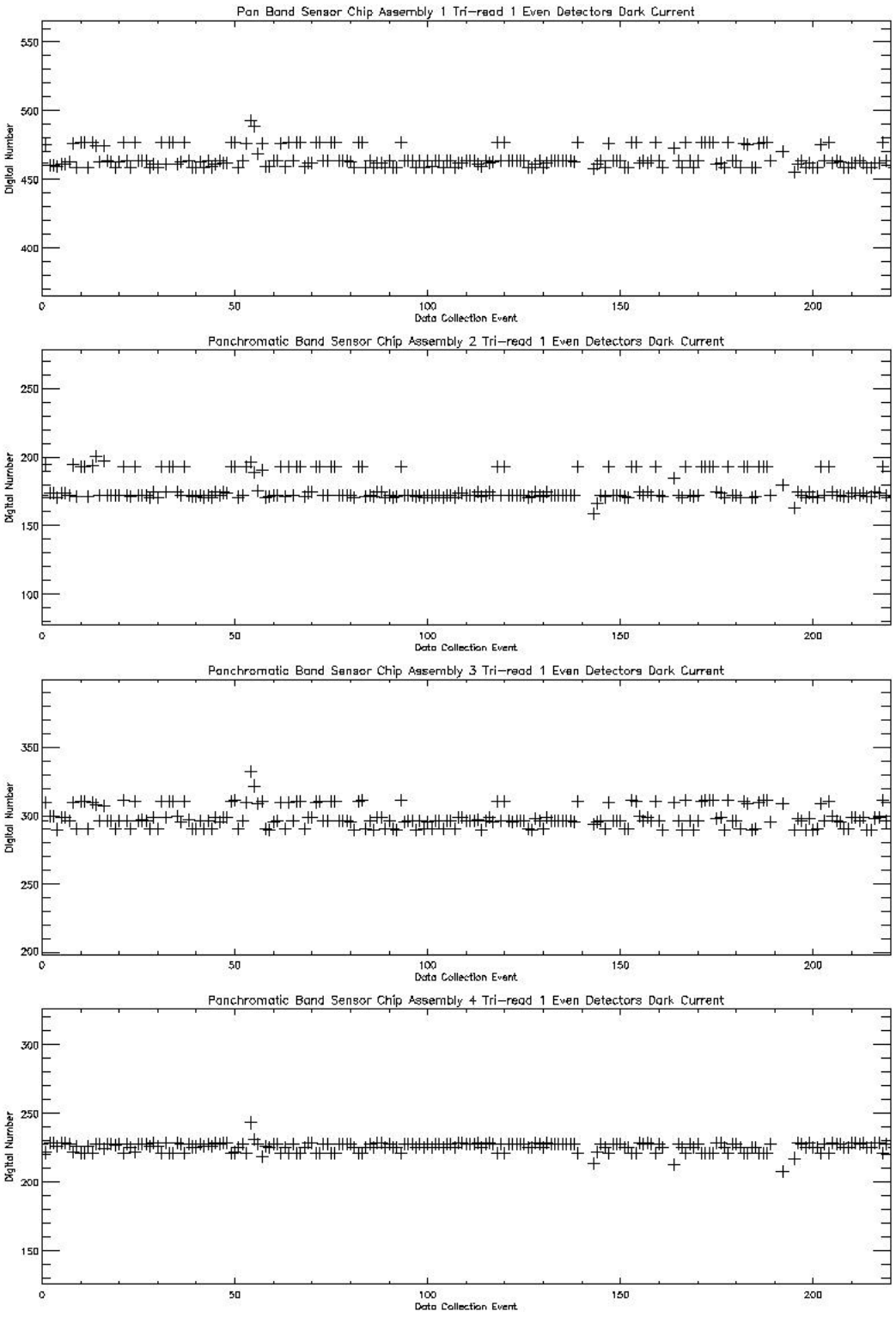

Figure 32: Dark current trending for Panchromatic Band tri-read #1 even detectors. Detector outgassing occurred near DCE 55, 140, 160, 190, and 219.

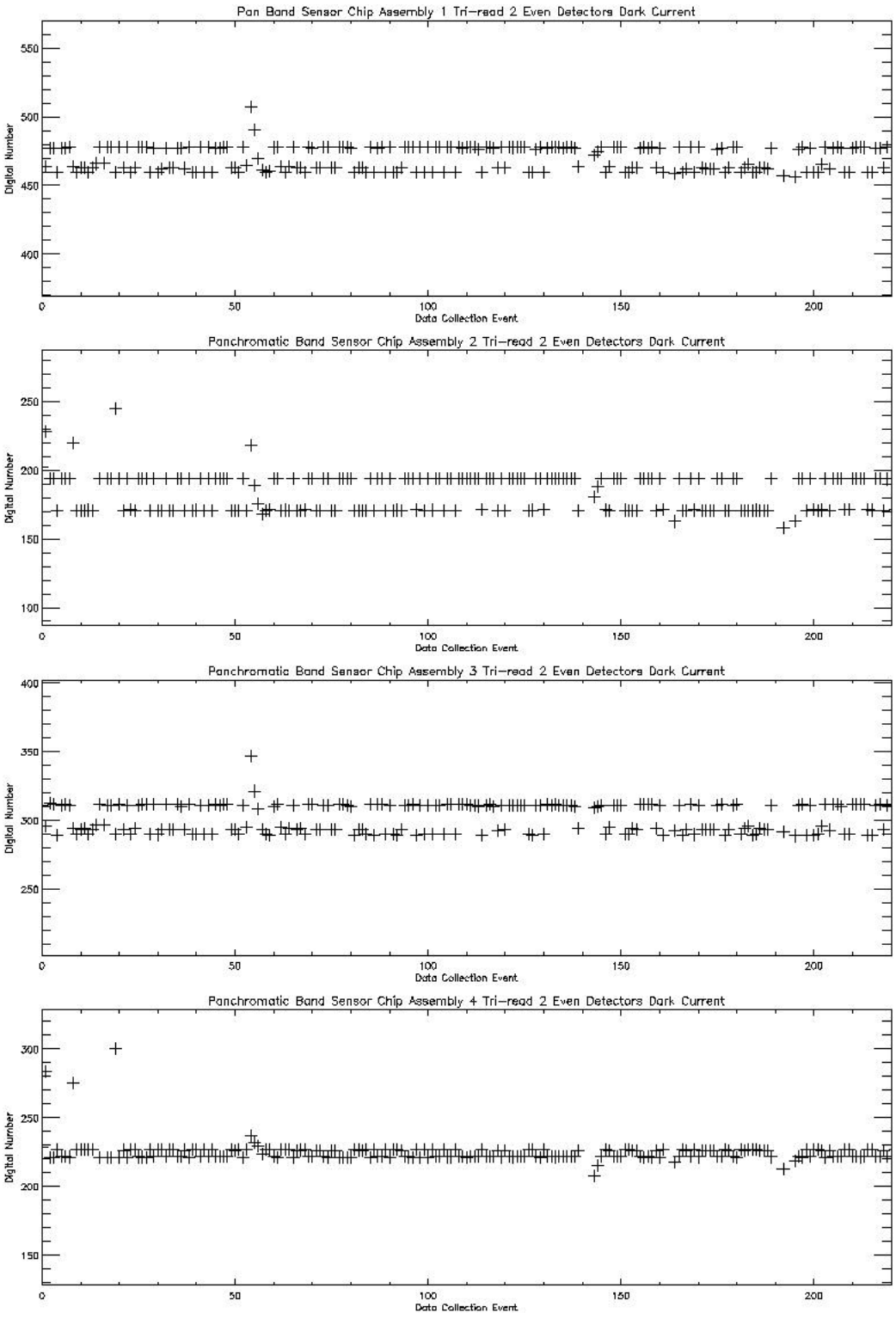

Figure 33: Dark current trending for Panchromatic Band tri-read #2 even detectors. Detector outgassing occurred near DCE 55, 140, 160, 190, and 219.

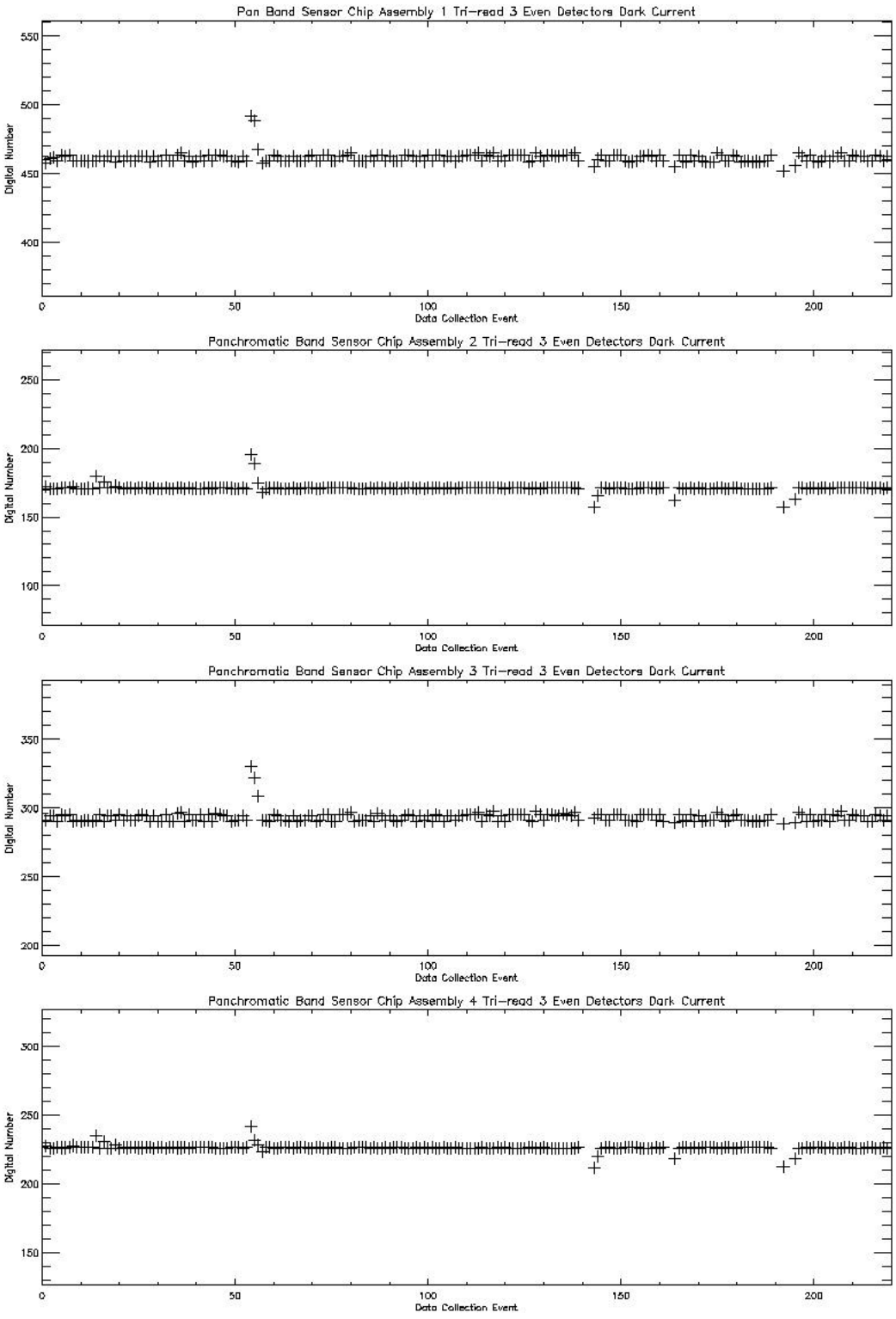

Figure 34: Dark current trending for Panchromatic Band tri-read #3 even detectors. Detector outgassing occurred near DCE 55, 140, 160, 190, and 219.

Table 3: Dark Current Trending Statistics

Band	SCA	Preflight Mean (Digital Number)	Flight Mean (Digital Number)	Flight Std. Deviation (Digital Number)
1P	1E	238.0	247.4	9.6
1P	1O	248.0	256.0	6.3
1P	2E	290.1	296.1	6.0
1P	2O	282.6	290.1	9.2
1P	3E	315.7	322.8	8.4
1P	3O	321.9	328.0	5.5
1P	4E	251.6	255.2	3.3
1P	4O	246.1	250.0	4.8
1	1E	248.2	249.3	1.2
1	1O	261.8	263.4	0.2
1	2E	318.2	320.5	0.6
1	2O	285.0	286.3	1.3
1	3E	277.7	277.1	1.1
1	3O	297.3	297.3	0.2
1	4E	257.0	257.6	0.2
1	4O	246.1	246.8	0.6
2	1E	259.5	260.5	0.1
2	1O	262.7	263.5	0.1
2	2E	292.0	294.2	0.6
2	2O	306.0	308.8	0.6
2	3E	263.6	263.3	0.2
2	3O	277.8	277.6	0.2
2	4E	257.4	258.0	0.2
2	4O	686.7	686.7	0.2
3	1E	256.9	257.7	0.1
3	1O	277.3	277.9	0.2
3	2E	283.8	285.6	0.6
3	2O	298.0	300.4	0.6
3	3E	625.2	626.2	0.3
3	3O	293.4	300.4	0.6
3	4E	261.6	262.6	0.2
3	4O	256.3	257.2	0.2
4	1E	258.6	257.1	5.8
4	1O	254.3	252.6	6.7
4	2E	292.5	289.2	7.3
4	2O	289.4	287.5	5.9
4	3E	299.9	297.7	5.1
4	3O	305.0	302.8	6.0
4	4E	255.3	255.9	3.4
4	4O	240.4	240.7	2.9
4P	1E	241.5	240.0	6.7
4P	1O	262.6	260.6	6.8
4P	2E	300.6	296.8	7.4
4P	2O	304.8	301.1	7.4
4P	3E	301.0	298.2	6.1
4P	3O	314.5	301.1	7.4
4P	4E	258.9	259.1	3.4
4P	4O	246.8	247.2	3.3

5P	1E	405.9	464.0	26.2
5P	1O	361.7	396.8	17.2
5P	2E	385.9	429.0	18.9
5P	2O	377.6	435.9	23.7
5P	3E	283.8	264.1	6.0
5P	3O	269.8	246.7	6.0
5P	4EQ1	282.7	300.1	7.1
5P	4EQ2	263.4	261.9	3.1
5P	4EQ3	403.8	395.7	4.6
5P	4EQ4	509.7	519.2	4.0
5P	4OQ1	301.1	332.4	11.1
5P	4OQ2	285.4	289.5	3.7
5P	4OQ3	426.5	426.7	3.4
5P	4OQ4	510.5	528.4	4.9
5	1E	307.7	314.8	7.6
5	1O	293.5	312.7	9.9
5	2E	347.9	346.6	9.5
5	2O	340.0	333.1	8.2
5	3E	261.2	248.6	5.6
5	3O	272.1	272.7	7.9
5	4EQ1	276.3	278.6	4.7
5	4EQ2	281.4	281.5	4.5
5	4EQ3	441.0	450.3	4.3
5	4EQ4	535.8	542.0	4.6
5	4OQ1	270.0	269.7	4.0
5	4OQ2	272.4	269.2	3.1
5	4OQ3	406.4	409.5	3.2
5	4OQ4	465.6	470.6	3.9
7	1E	382.3	457.5	22.1
7	1O	235.7	325.7	31.2
7	2E	242.3	369.8	30.1
7	2O	389.1	461.1	17.9
7	3E	300.1	290.6	8.4
7	3O	140.2	137.8	8.8
7	4EQ1	164.5	238.7	18.9
7	4EQ2	181.2	214.1	9.0
7	4EQ3	371.1	395.9	6.9
7	4EQ4	483.0	559.7	15.6
7	4OQ1	318.4	368.8	12.2
7	4OQ2	359.6	379.5	8.4
7	4OQ3	599.1	616.4	6.5
7	4OQ4	726.7	790.8	13.7
PAN	1ET1	465.7	465.5	6.8
PAN	1ET2	479.2	469.8	8.2
PAN	1ET3	465.3	461.2	2.2
PAN	1OT1	176.6	176.4	8.4
PAN	1OT2	197.2	188.1	9.0
PAN	1OT3	175.9	172.0	2.2
PAN	2ET1	172.4	177.7	9.3
PAN	2ET2	193.8	186.9	8.0
PAN	2ET3	171.5	171.1	0.8
PAN	2OT1	381.8	383.3	7.7
PAN	2OT2	396.2	388.8	8.7

PAN	2OT3	378.5	379.7	2.1
PAN	3ET1	295.8	298.9	7.3
PAN	3ET2	311.3	301.8	9.8
PAN	3ET3	295.4	293.0	2.3
PAN	3OT1	74.0	77.6	8.6
PAN	3OT2	91.9	84.2	8.4
PAN	3OT3	67.5	67.6	0.9
PAN	4ET1	226.3	225.9	2.8
PAN	4ET2	229.5	228.4	2.7
PAN	4ET3	224.5	226.2	0.9
PAN	4OT1	448.8	448.6	2.4
PAN	4OT2	451.4	446.3	1.4
PAN	4OT3	447.3	448.7	0.5

5 Discussion

The magnitude and repeatability of the EO-1 Advanced Land Imager focal plane noise were excellent during the first sixty days in orbit. The magnitudes presented in Table 2 are consistent with those calculated during pre-flight calibration of the instrument[6]. The trending indicates little change in noise levels throughout this period, except during times when the focal plane was being warmed-up for outgassing.

The magnitude of the ALI focal plane dark current was as expected during the first sixty days in orbit. The magnitudes presented in Table 3 are consistent with those calculated during pre-flight calibration of the instrument[6]. Band 2 SCA4 odd detectors and Band 3 SCA 3 even detectors have increased dark current levels compared to the corresponding even and odd detectors respectively. This is due to the influence of previously identified leaky detectors in these bands. Additionally, all SWIR bands exhibit enhanced dark current levels for a region of SCA 4 that is associated with a previously identified 'hot spot' in the focal plane.

Analysis of dark current data indicates excellent stability of all dark current levels within a given observation. However, dark current level variability as high as 30 digital numbers for Bands 1p, 4, 4p, 5p, 5, 7, and the Panchromatic band has been observed from one observation to another and is not well understood at this time. A small (20-50 digital numbers) increase in dark current is also observed in Bands 5p and 7 over the coarse of the first 150 DCEs. More frequent outgassing (once per week) since then has reduced this drift to less than 10 digital numbers.

Additional changes in noise and dark current levels are observed during times when the focal plane was being heated for outgassing. However, even during these periods, all Visible and Near Infrared bands (1p, 1, 2, 3, 4, 4p) and the Panchromatic Band indicate little change in detector dark current levels. This is undoubtedly the result in differing dark current characteristics between the silicon (VNIR) and HgCdTe (SWIR) detector materials.

The results presented here will serve as baselines for noise and dark current trending during the remainder of the EO-1 mission.

6 References

1. J. A. Mendenhall et al., "Earth Observing-1 Advanced Land Imager: Instrument and Flight Operations Overview," MIT/LL Project Report EO-1-1, 23 June 2000.
2. D. E. Lencioni, C. J. Digenis, W. E. Bicknell, D. R. Hearn, J. A. Mendenhall, "Design and Performance of the EO-1 Advanced Land Imager," *SPIE Conference on Sensors, Systems, and Next Generation Satellites III*, Florence, Italy, 20 September 1999.
3. W. E. Bicknell, C. J. Digenis, S. E. Forman, D. E. Lencioni, "EO-1 Advanced Land Imager," *SPIE Conference on Earth Observing Systems IV*, Denver, Colorado, 18 July 1999.
4. C. J. Digenis, D. E. Lencioni, and W. E. Bicknell, "New Millennium EO-1 Advanced Land Imager," *SPIE Conference on Earth Observing Systems III*, San Diego, California, July 1998.
5. D. E. Lencioni and D. R. Hearn, "New Millennium EO-1 Advanced Land Imager," *International Symposium on Spectral Sensing Research*, San Diego, 13-19 December 1997.
6. J. A. Mendenhall et al., "Earth Observing-1 Advanced Land Imager: Dark Current and Noise Characterization and Anomalous Detectors," MIT/LL Project Report EO-1-5, 23 February 2001.

This work was sponsored by NASA/Goddard Space Flight Center under U.S. Air Force, Contract F19628-95-C-0002.

Opinions, interpretations, conclusions, and recommendations are those of the authors and are not necessarily endorsed by the United States Air Force.